CLEAN WATER

WATER POLLUTION CONTROL RESEARCH SERIES ● 14010 FNQ 02/72

Electrochemical Treatment of Acid Mine Waters

U.S. ENVIRONMENTAL PROTECTION AGENCY

WATER POLLUTION CONTROL RESEARCH SERIES

The Water Pollution Control Research Series describes the results and progress in the control and abatement of pollution in our Nation's waters. They provide a central source of information on the research, development and demonstration activities in the Environmental Protection Agency, through inhouse research and grants and contracts with Federal, State, and local agencies, research institutions, and industrial organizations.

Inquiries pertaining to Water Pollution Control Research Reports should be directed to the Chief, Publications Branch (Water), Research Information Division, R&M, Environmental Protection Agency, Washington, D.C. 20460.

ELECTROCHEMICAL TREATMENT OF ACID MINE WATERS

by

Tyco Laboratories, Inc.

Bear Hill

Waltham, Massachusetts 02154

for the

ENVIRONMENTAL PROTECTION AGENCY

Project No. 14010 FNQ

Contract No. 14-12-859

February 1972

For sale by the Superintendent of Documents, U.S. Government Printing Office, Washington, D.C. 20402 - Price $1.00

EPA Review Notice

This report has been reviewed by the Environmental Protection Agency and approved for publication. Approval does not signify that the contents necessarily reflect the views and policies of the Environmental Protection Agency nor does mention of trade names or commercial products constitute endorsement or recommendation for use.

ABSTRACT

Experimental and analytical evaluations of the direct electrochemical oxidation of ferrous acid mine drainage (AMD) have shown that this approach is economically superior to present lime treatment and aeration methods. Through the use of a packed bed electrode, the size of the oxidation reactor has been reduced to a stage where the capital investment required for this equipment can be recovered by cost reductions in latter treatment stages. These cost savings include:

1. Neutralization with cheaper limestone rather than lime

2. A reduction in sludge settling time due to the better properties of limestone sludges

3. Reduction of sludge disposal volume.

As a bonus, electrolytic hydrogen, produced during electrochemical oxidation, should be economically recoverable at high AMD treatment rates.

Preliminary economic estimates of total treatment costs indicate a cost range from 11¢ to 72¢/1000 gal, exclusive of hydrogen credits. These costs are much less than those of present treatment approaches which appear to have expense rates of from 20¢ to $ 2.00/1000 gal treated. In the particular case of a badly polluted stream containing 2000 mg/ℓ of $CaCO_3$ acidity, the total treatment cost of 31¢/1000 gallon for the electrochemical oxidation approach is less than the reagent cost alone (~ 35¢/1000 gal) for conventional lime treatment.

This report was submitted in fulfillment of Project Number 14010FNQ and Contract Number 14-12-859 under the sponsorship of the Water Quality Office, Environmental Protection Agency.

Contents

Figures

Figures (Cont)

Figures (Cont)

Tables

SECTION I

CONCLUSIONS

The following is a list of those conclusions which are relevant to the development of a practical electrochemical process for treating AMD.

1. The anodic oxidation of Fe^{2+} to Fe^{3+} takes place on a carbon electrode at a mass transport limited rate. The oxidation region is about 0.80 V in extent. The potential plateau for this process is shifted to more positive values by increasing the Fe^{3+} concentration although this shift (<0.2 V) is not sufficient to cause problems in an operational system.

2. Excessive oxidation (high positive potentials) at the carbon electrode inhibits the Fe^{2+} oxidation. In a practical reactor, however, such high positive potentials will not be reached.

3. Hydrogen evolution occurs on a polished 316 stainless steel cathode (in deaerated 0.01, 0.02M H_2SO_4) at potentials more negative than 0.5 V (SCE). These currents are not diffusion limited but are controlled by a slower electrochemical kinetic step.

4. The cathode in 0.02M H_2SO_4 is passivated by an oxide film at potentials more positive than -0.04 V. This film is removed only at potentials more negative than -0.90 V, the normal operating region of the cathode.

5. The diffusion limited back reduction of Fe^{3+} to Fe^{2+} occurs at potentials more negative than -0.15 V.

6. Soluble ferric iron is reduced to the metal on a 316 stainless steel cathode in 0.02M H_2SO_4 at potentials $\leq$-1.0 V. Large currents from H_2 evolution can be supported before iron deposition occurs.

7. A highly selective membrane is available which will prevent the penetration of Fe^{3+} specie while possessing acceptable ohmic and structural characteristics.

8. Smooth carbon electrodes show a slow degradation in performance as the result of poisoning by soluble species. The degradation is enhanced in AMD water prepared from waste coal. This effect has not been detected with porous carbon electrodes.

These results were then used as the basis for an experimental and engineering evaluation of the following prototype electrochemical reactors: (a) fluidized bed, (b) packed bed, (c) annular flow.

Of these three the packed bed electrode gave rise to the smallest and hence most economical configuration.

An evaluation of process economics, using a packed bed reactor, indicated total treatment costs in the range of 11¢ to 72¢/1000 gal, compared to present costs of 20¢ to $2.00/1000 gal. Additional cost savings are possible from the sale of electrolytic hydrogen. Because of transportation and collection costs, these savings would be realized when handling large volumes of highly polluted AMD water.

As compared with alternative oxidation methods, the electrochemical process is free of the safety hazards associated with radioisotope-induced oxidation and should as well be free of the temperature sensitivity associated with biological oxidation methods.

SECTION II

RECOMMENDATIONS

The experimental work discussed in this report has amply demonstrated the technical feasibility of electrolytically oxidizing ferrous iron in AMD to ferric. An evaluation of system economics indicates potential cost benefits are to be realized.

The following are recommended:

1. This process be scaled up to the construction of a full sized packed bed module

2. The reactor be operated first in the laboratory and next in field on actual AMD

3. The data so acquired be used to obtain a more precise evaluation of process economics

4. The applicability of the process be evaluated in terms of specific treatment sites.

SECTION III

INTRODUCTION

Waters which accumulate in mines, and waters draining from mines and exposed coal formations represent a significant pollution problem which has been receiving increased attention. Such acid mine drainage (AMD) is typically highly acidic (pH 2 to 3) and contains significant quantities of dissolved salts (principally iron sulfates). Although there are significant variations, this dissolved iron exists mostly in the ferrous state.

Chemical AMD treatment methods typically involve neutralization, using low cost materials such as limestone or lime, concurrent with an aeration step to oxidize the ferrous iron to the ferric state. This oxidation is necessary in order to avoid the high pH required for ferrous iron precipitation.

Air oxidation is a relatively slow process which is highly dependent on the pH of the water and on the efficiency of the aeration system. Significant oxidation rates do not occur until the solution becomes neutral or basic (pH>7). Therefore, high ferrous AMD is typically neutralized with more expensive lime rather than limestone which is too weak a base to produce a pH above 5.5.

The resulting voluminous sludge (typically less than 5% solids) is separated from the bulk stream and stored. The high residual alkalinity of the sludge produced with the lime neutralization process adds to the disposal problems since further leaching of the sludge piles is likely. In addition, close control over the neutralization step is needed to avoid overtreatment with the resultant alkaline stream flow.

Alternative oxidation processes which would proceed rapidly in a highly acid solution have, of course, been considered. Direct chemical treatment with nonpolluting oxidants, e.g., hydrogen peroxide, sodium peroxide, or ozone, involve intolerably high reagent costs for the flow rates that are involved.

Biological techniques, in addition to requiring an aeration step, proceed relatively slowly, and are adversely affected by temperature. Another possible approach is electrochemical oxidation. An acid mine water, containing on the average 500 mg/l of Fe^{2+} and 1000 mg/l H^+ and variable amounts of aluminum, calcium and manganese, is an electrolytically conducting solution. As such, it is capable of electrolysis without resort to additional salt additives. The electrochemical reaction :

$$Fe^{2+} \rightarrow Fe^{3+} + e^-$$

would take place at an inert (nonconsumable) anode. Concurrently, on an inert cathode, the reaction:

$$H^+ + e^- \rightarrow 1/2\ H_2$$

would take place, resulting in the generation of 1/2 mol of hydrogen gas for every mol of iron that is oxidized.

This report describes the technical and economic evaluation of an AMD treatment process based on these reactions.

It will be shown that major cost savings for the entire process can accrue from the subsequent treatment of nearly 100% ferric mine water produced by the electrochemical oxidation step. Precipitation of Fe^{3+} with cheaper limestone produces a denser sludge (10 to 20% solids) with a faster settling time. Thus, in addition to savings in reagent costs, capital and operating outlays for sludge separation and sludge disposal can be lower than when lime is used as the neutralizing agent.

In essence, the costs of the increased capital investment required for the direct electrochemical oxidation of ferrous mine waters will be defrayed by lesser capital investment and operating expenses in later treatment stages. Such a treatment process would have the additional attraction of generating by-product electrolytic hydrogen. It will be shown that, in certain situations, this hydrogen can be sold to further defray treatment costs.

SECTION IV

BASIC ELECTROCHEMISTRY

Upon the electrolysis of acid mine drainage water, the following electrochemical processes are possible for the major soluble ionic species:[1]

1. At the negative electrode (the cathode):

$$2H^+ + 2e^- \rightleftharpoons H_2 \qquad E = -0.35\ V \qquad (1)$$

$$Fe^{2+} + 2e^- \rightleftharpoons Fe \qquad E = -0.79\ V \qquad (2)$$

$$Fe^{3+} + e^- \rightleftharpoons Fe^{2+} \qquad E = +0.52\ V \qquad (3)$$

2. At the positive electrode (the anode):

$$Fe^{2+} \rightleftharpoons Fe^{3+} + e^- \qquad E = +0.52\ V \qquad (3a)$$

$$2H_2O \rightleftharpoons O_2 = 4H^+ + 4e^- \qquad E = +0.88\ V \qquad (4)$$

$$2H_2O \rightleftharpoons H_2O_2 + 2H^+ + 2e^- \qquad E = +1.41\ V \qquad (5)$$

$$2HSO_4^- \rightleftharpoons S_2O_8^{=} + 2H^+ + 2e^- \qquad E = +1.8\ V \qquad (6)$$

$$2SO_4^{=} \rightleftharpoons S_2O_8^{=} + 2e^- \qquad E = +1.7\ V \qquad (7)$$

The electrical potentials listed are thermodynamic values versus a saturated calomel reference electrode (SCE) and apply for concentrations of 0.02 N. The sign (+ or -) is that which results from the use of the standard reduction potential convention for half-cell reactions.

The desired anodic process is reaction 3a and the desired cathodic process is reaction 1. All other processes are to be considered parasitic for the development of a viable AMD treatment.

For all practical purposes, it is possible to disregard reactions 5 through 7 since these occur at potentials more positive than those readily accessable in dilute aqueous electrolytes. The current (reaction rate)-potential dependencies of the remaining reactions were determined experimentally.

EXPERIMENTAL

AMD water varies in Fe^{2+} concentration and pH[2]; 0.02M in Fe^{2+} and in H_2SO_4 was taken as representative. In the initial studies, the experimental conditions were simplified by using pure $FeSO_4$ ($FeSO_4 \cdot 7\ H_2O$, Fisher Scientific Co.) and pure H_2SO_4 (suprapure grade, Brinkmann Instruments, Westbury, N.Y.). Subsequently, the results were confined in "synthetic" AMD water produced in the laboratory by draining water through waste coal. The characteristics of this water were described in the Final Report for Project 14010 DLI, contract 14-12-560.

Normally this effluent solution from the waste coal was cloudy yellowish brown in color and varied in total soluble iron concentration from $\sim 4 \times 10^{-3}$ M to $\sim 2 \times 10^{-2}$ M (both Fe^{2+} and Fe^{3+}). The solution was generally pH 2.7. When these water samples were left for extended periods of time, the Fe^{2+} concentration usually decreased and Fe^{3+} increased, presumably from oxidation of the former by dissolved O_2. (The participation of bacteria in this process was not studied.) Thus, over a 5-day period, initial concentrations of 1.7×10^{-2}M Fe^{2+} and 1.2×10^{-2}M Fe^{3+} changed to 1.4×10^{-2}M Fe^{2+} and 1.3×10^{-2}M Fe^{3+}. Some iron was apparently lost through precipitation during the period. Ferrous and ferric concentrations were determined for this and subsequent experiments by the standard dichromate techniques using a diphenylamine sulfonate indicator.[18]

In most experiments, this "synthetic AMD" was first centrifuged for 10 min before use, in order to remove solid residues. This treatment caused only a small drop in concentration of both Fe species; the solution was then clear. However, a yellowish brown residue settled out in the electrochemical cell over a period of days. Similarly when the solutions were passed through a 0.45-μ Millipore filter, the cloudiness was removed but again a light yellow residue settled out in the deaerated cell over several days. This latter treatment also slightly reduced the concentration of both Fe species in solution.

The values for both Fe^{2+} and also Fe^{3+} in these solutions are somewhat greater than might normally be found in AMD in streams,[3] i.e., after natural dilution. In some experiments, therefore, this synthetic AMD was diluted with 0.02M H_2SO_4 before use.

The measurements of solution conductivities were carried out using a conductivity bridge (model no. R.C. 16B2, Industrial Instruments, Inc., Cedar Grove, N.J.). Conductivities of a series of solutions containing 10^{-2} to

10^{-6} M Fe^{2+} in 0.02 and 0.01M H_2SO_4 were measured. The presence of Fe^{2+} had minimal effect on the conductivities of the solutions. Typical values ranged from 104.6 ohm-cm (10^{-6} M Fe^{2+} in 0.02M H_2SO_4) to 183.5 ohm-cm (10^{-6} M Fe^{2+} in 0.01M H_2SO_4).

Carbon was selected as the anode since it is inexpensive, can be obtained in tubular form, is very resistant to chemical attack, and has a relatively wide potential range over which it is electrochemically stable[3] (i.e., does not evolve O_2, H_2, or dissolve). As cathode, 316-stainless steel rather than pure iron was chosen, since stainless steel is more resistant to corrosion in dilute acids.

Initial experiments on a carbon anode were aimed at confirming its stability under applied potential, and determining the potential range over which Fe^{2+} can also be oxidized. In the latter context, it was necessary to determine the potential region in which Fe^{2+} is oxidized at a mass transport limited rate, i.e., in the absence of any electron transfer or other limitations. A rotating disk electrode[5] was used in these studies. This configuration is particularly useful since the hydrodynamic boundary layer setup is well characterized.[5] Thus, in a purely mass transport limited situation, currents for Fe^{2+} oxidation can be calculated at given rotation speeds of the assembly, using the equation derived by Levich:[5]

$$i_{lim} = 0.62\, nFD^{2/3}\, \pi\, r^2\, \upsilon^{-1/6}\, \omega^{1/2}\, c_b \qquad (8)$$

where
- n = number of electrons involved in the process
- F = the Faraday constant
- D = diffusion coefficient (cm^2/sec)
- r = radius of the disk (cm)
- υ = kinematic viscosity of the solution ($cp/cm^3/gm$)
- ω = rotation speed of the disk (rad/sec)
- c_b = bulk concentration of reactive species (mol/l)
- i_{lim} = limiting current (mA)

An overall view of the rotating disk electrode setup is shown in Fig. 1. The equipment consists of a sturdy stand on which a 1/15-hp Bodine motor and a precision ball bearing for the 0.025 in. rotating shaft were mounted. The motor speed was controlled by a Minarik speed control (SL-52). The coupling of the motor and the electrode shaft was accomplished by a nonslip belt. The rotation rate of the electrode was continuously monitored by frequency modulation resulting from magnetic coupling of an electromagnet with an iron gear mounted on the rotating shaft. This signal was amplified and displayed on a frequency counter (Hewlett Packard model no. 5221A). Electrical contact to the disk electrode was accomplished through a mercury pool in the top of the rotating shaft.

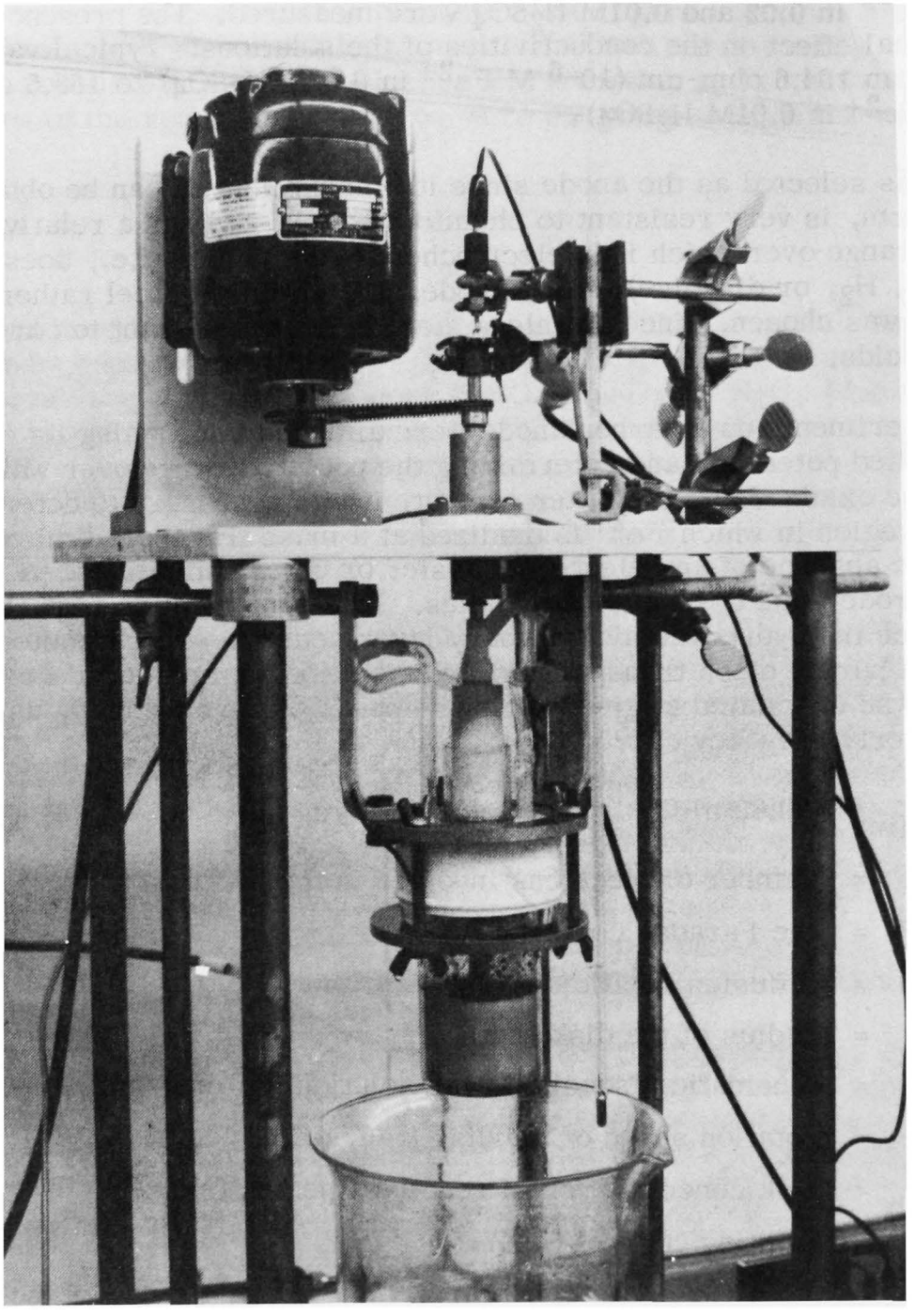

Fig. 1. Overall view of rotating disk assembly

The electrochemical cell was made of a 50-mm O-ring joint with a 30 mm thick Teflon cover. The Teflon cover contained tapered holes to accommodate a liquid seal in the center with a 29/40 standard tapered joint surrounded by four 10/30 joints for gas inlet (N_2) and outlet as well as the counter- (platinum) and reference electrodes (calomel). A Teflon bell was fixed to the rotating shaft. Mercury was used as sealant liquid to prevent O_2 from contacting the solutions.

Fig. 2 is a diagram of the actual electrode. The main feature of this electrode is the vitreous carbon anode (Atomergic Chemetals Co., 584 Mineola Avenue, Carle Place, L.I., N.Y.), which is press-fitted into hot Teflon and contacts the upper mercury pool via a simple spring. A rotating disk electrode was constructed inhouse from 316-stainless steel rod.

The electronic equipment employed was a potentiostat (Wenking model no. 61TRS, Brinkmann Instruments, Westbury, N.Y.) supplying ±1 A at ±15 V with a rise time of $\sim 10^{-5}$ sec. This was used to control the potential between the calomel reference and carbon anode using a platinum counterelectrode. A Tyco-built function generator (TLI no. 661207) was used to apply a linear voltage sweep (1 V/min and 0.1 V/min) to the system, and current-voltage curves were recorded on an x-y recorder (model no. R-100, Houston Omnigraphic Corp., Bellaire, Texas). Voltage drop (i-R) in the system was measured on an oscilloscope (Tektronix type 561A with 2A63 and 2B67 plug-ins) by interrupting an applied constant current. IR was compensated for during the measurements by a suitable amplifier setup. Potentials were measured and are reported versus an SCE.

ANODIC OXIDATION OF FERROUS IRON

The basis of this AMD treatment concept is being able to oxidize electrochemically ferrous iron to ferric at a rapid rate, i.e., at a rate limited only by the mass transport of ions to the electroactive surface. Specifically it was necessary then to determine:

1. In what potential region was the anodic oxidation of ferric iron diffusion limited

2. At what potential did the oxidation of water to O_2 occur

3. In which potential region the carbon electrode itself was stable.

Solutions employed were: (1) 0.02M H_2SO_4 to examine the limits of stability of the carbon anode in these solutions, and (2) 0.02M Fe^{2+} to 5×10^{-4} M Fe^{2+}

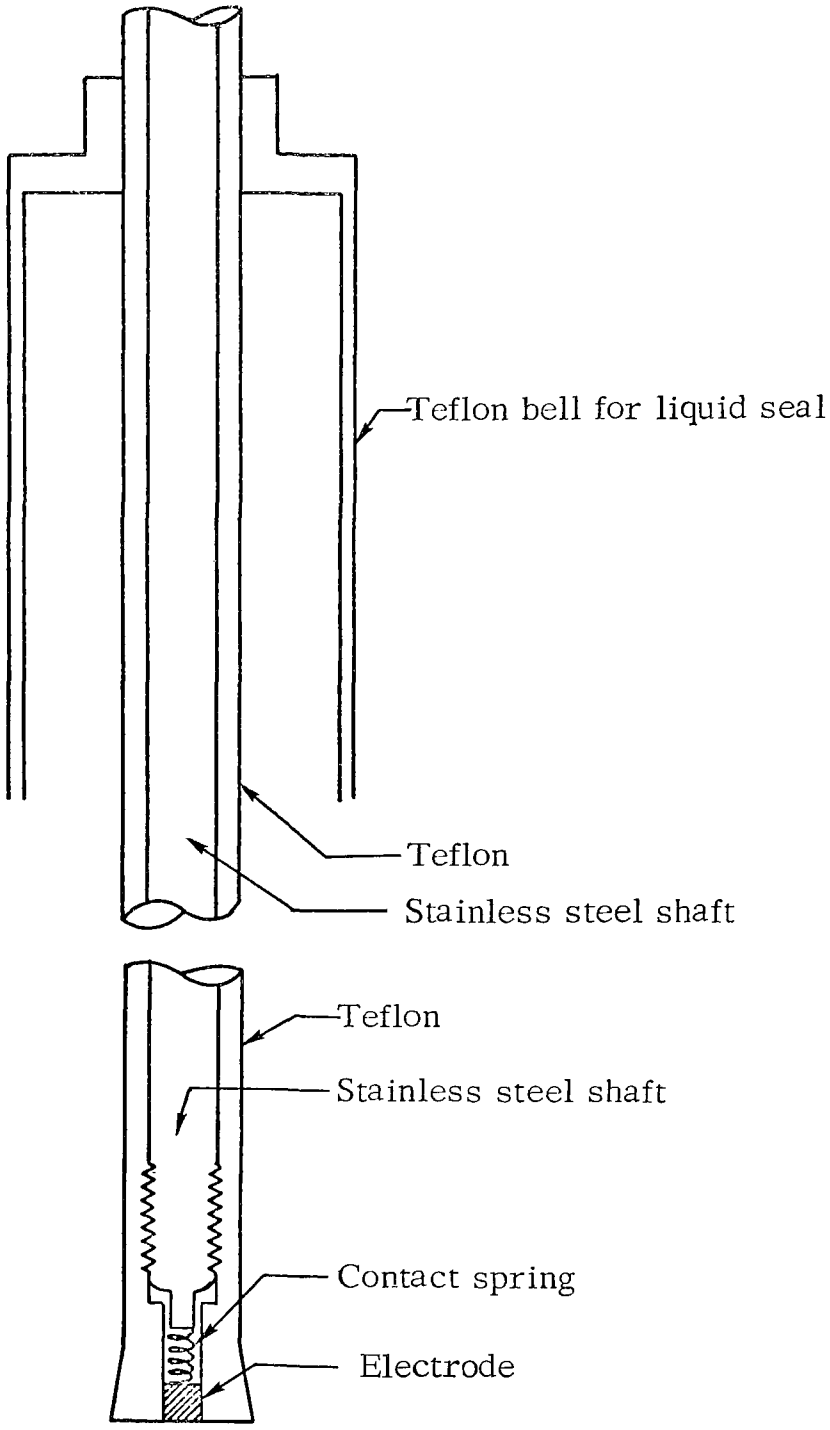

Fig. 2. Schematic of rotating disk electrode

in 0.02M H_2SO_4 to examine the oxidation of Fe^{2+} to Fe^{3+} at the anode. Solutions were deaerated with N_2 prior to scanning the electrode. Rotation speed of the electrode was varied from 3.0 to 50.6 rps.

Fig. 3 shows a typical voltage scan (0.10 V.min) on a carbon anode in deaerated 0.02M H_2SO_4. At 0 V (SCE), a small (2-μA) negative current is observed which becomes positive and increases steadily (on scanning positive) until it reaches a value of +16 μA at 1.2 V (SCE). Above this potential, the current increases more rapidly with increase in E, corresponding to the onset of O_2 evolution (+1.2 V $\rightarrow$ +1.6 V SCE). The reverse scan from these potentials does not follow the forward one exactly, but remains slightly below it. The electrode is stable in the cathodic direction to -0.90 V (SCE), at which point H_2 is observed. The relatively high value of background current observed during the scan is attributed to the double layer charging process as E is increased, rather than from impurities in solution.

Solutions containing 0.01M Fe^{2+} were scanned between the general limits -1.2 V and +1.5 V (SCE). A typical sequence is shown in Fig. 4 where the detailed scan history was from -0.80 V held for 20 min, then immediately to +1.5 V. The reverse scan from +1.5 to 0 V was then carried out. Negative scans ($<$ 0.0 V) were completed at 1 V.min, while all the data in Fig. 3 were at 0.102 V/min. Electrode rotation speed was 23.4 rps.

On the reverse scan from +1.5 V, a prewave is in evidence. However, the figure shows clearly that no prewave is found on the forward scan to +1.5 V. It was found that, if the electrode was cycled between 0.0 V and +1.5 V, the prewave became more marked. If the electrode was cycled from 0 to -1.2 V and back again, or held at -0.8 V for 20 min before carrying out the scan to positive potentials ($>$ 1.2 V), then the prewave was not observed. Provided the electrode was not scanned beyond +1.2 V, the prewave did not reappear.

It was easily shown that this prewave was not to be due to solution impurities. It was necessary then to show that the prewave was, in fact, characteristic of a carbon anode solely, rather than some extraneous effect, and, more important did not necessarily result in a permanent degradation of the electrode. Therefore the experiment was repeated, but using a rotating platinum disk as anode; the electrochemical properties of this metal and its oxides are well established.

Fig. 5 shows the oxidation of 0.01M Fe^{2+} on a rotating Pt electrode in 0.02M H_2SO_4 using a scan speed of 0.102 V/min and a rotation speed of 23.4 rps. Also shown is the reverse scan on the electrode. The overall currents shown are greater than on the C-electrode, purely because of the greater area of the platinum electrode. What is most evident is the fact that the prewave is not found on platinum. Attempts to reproduce the phenomenon observed on the C-electrode by varying scan speed and rotation speed were not successful.

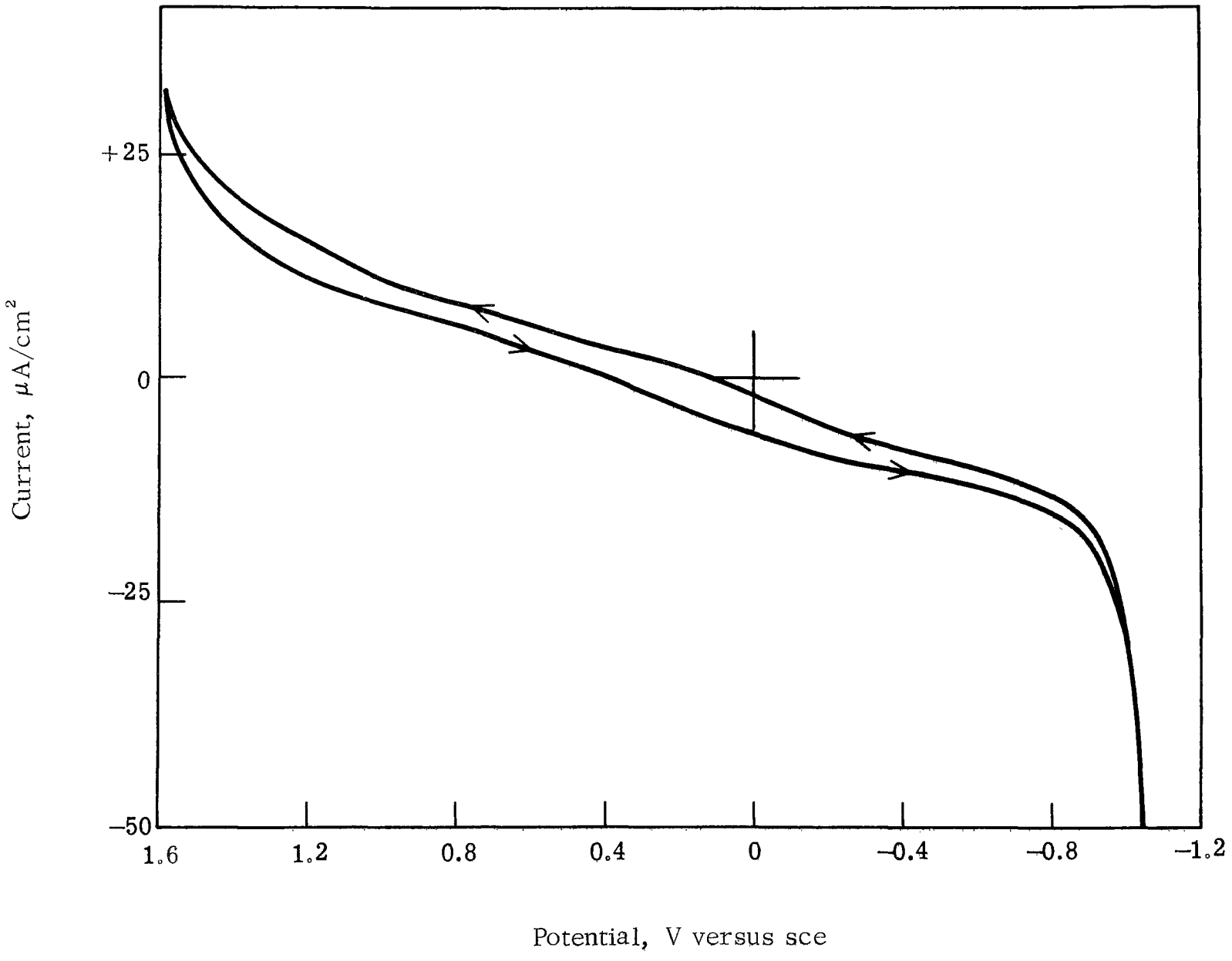

Fig. 3. Current-voltage scan on a vitreous carbon electrode in 0.02M H_2SO_4 at ambient temperature (scan rate = 0.10 V/min)

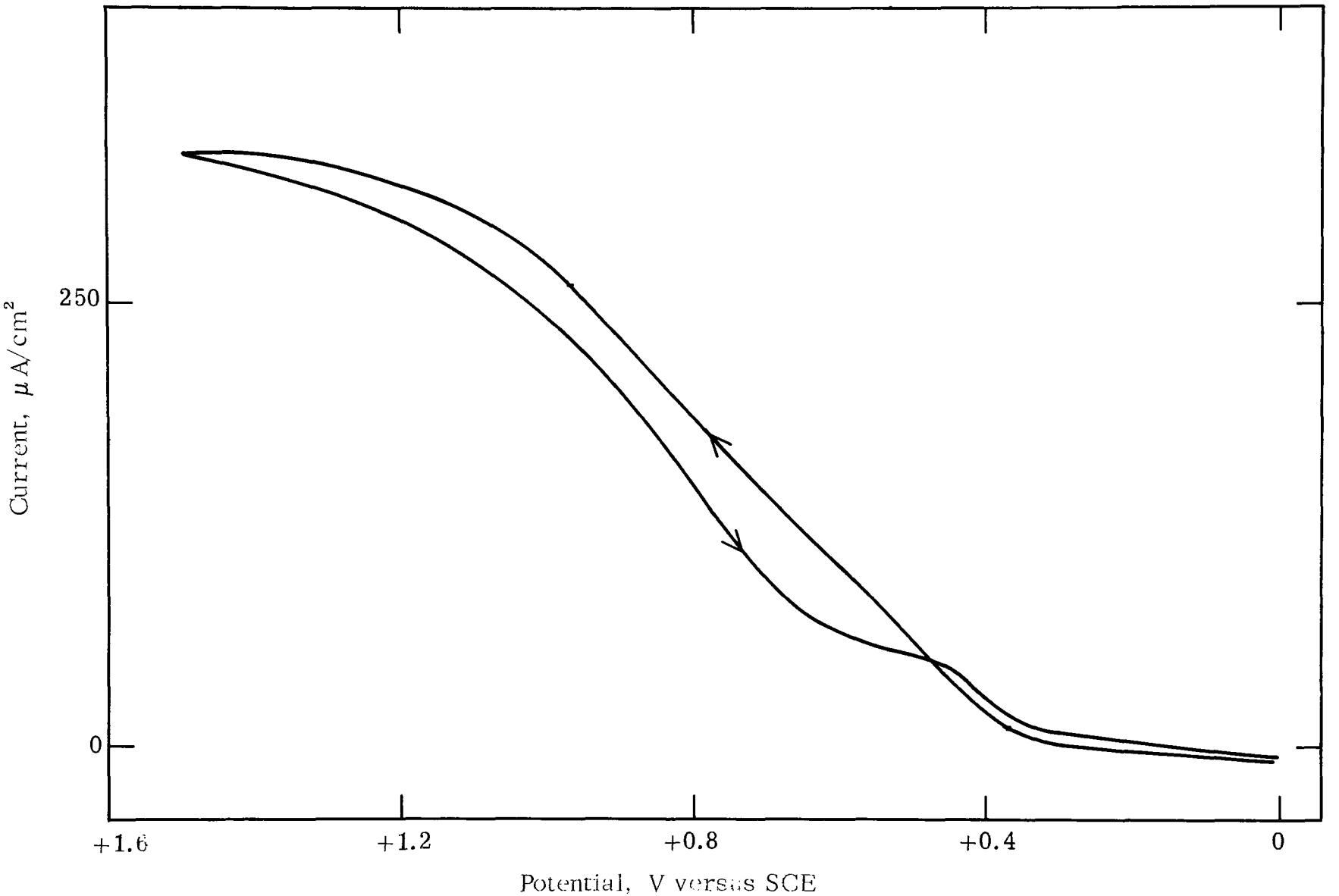

Fig. 4. Typical current-voltage scans to 1.5 V (SCE) on a vitreous carbon electrode in 0.02M H_2SO_4 containing 0.01M Fe^{2+} (scan rate = 0.10 V/min, rotation speed = 23.4 rps)

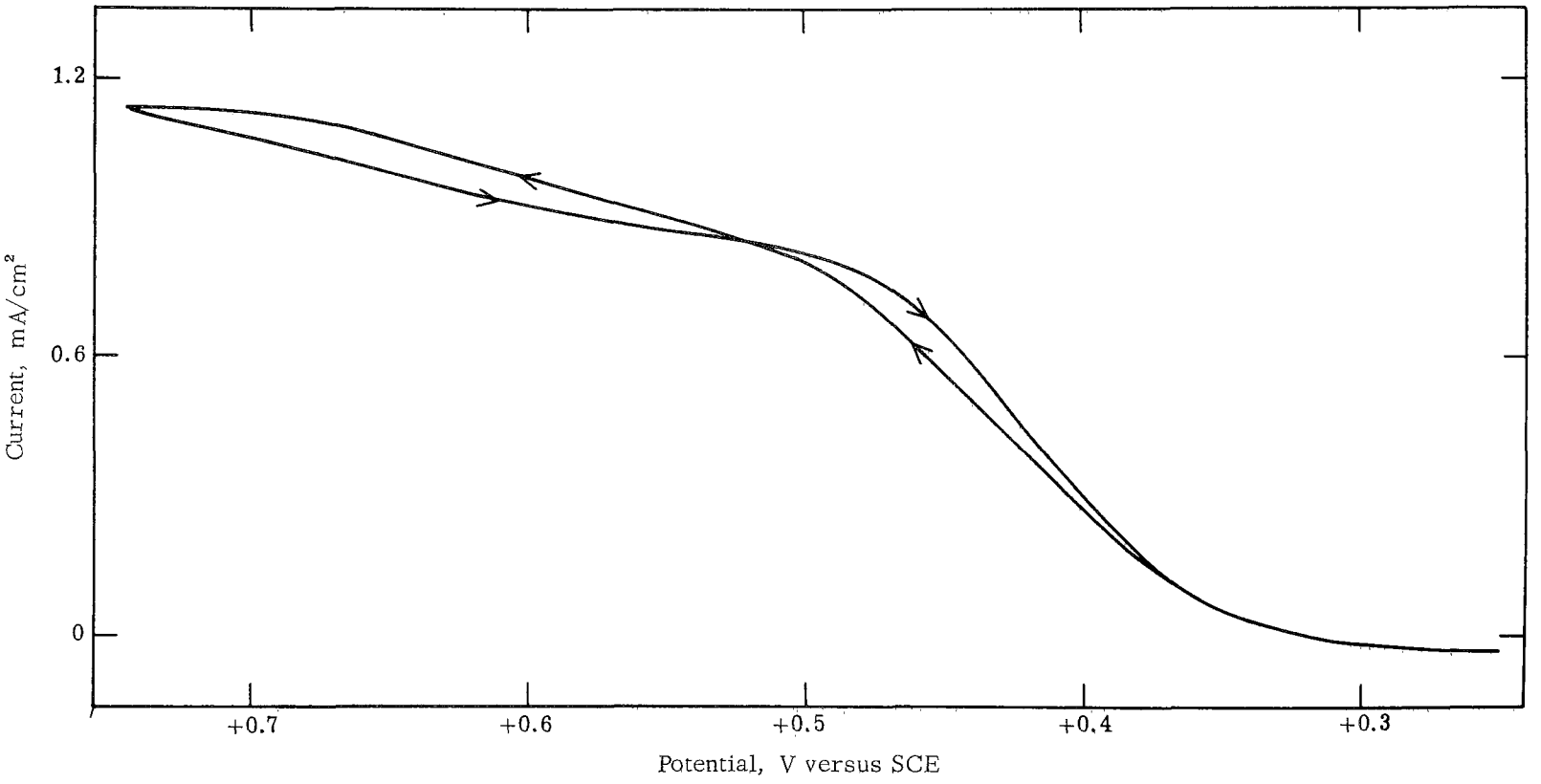

Fig. 5. Typical current-voltage scan to 0.75 V (SCE) on a platinum electrode in 0.02M H_2SO_4 containing 0.01M Fe^{2+} (scan rate = 0.10 V/min, rotation speed = 23.4 rps)

Basically, it was assumed that the wave was caused by a change in the nature of the electrode surface during scanning. The most likely change is the formation of a surface oxide at high positive potentials and it is known, at least for materials like platinum, that surface oxides inhibit the oxidation of Fe^{2+} to Fe^{3+}. Therefore, an attempt was made to induce the prewave by forming platinum oxide on the electrode. With our electrochemical system, in effect calibrated by this better established process, it would then be possible to interpret the data for carbon.

In Fig. 6 data equivalent to that in Fig. 5 are shown on a Pt electrode, except that in Fig. 6 the electrode was scanned out to +1.2 V (SCE) where an oxide is known to form on Pt.[6] (In Fig. 5, the scan was only made to +0.75 V (SCE) where little Pt - O is formed.[6]) Whereas the two plateaus in Fig. 5 almost coincide, those in Fig. 6 differ markedly. On the forward scan of Fig. 6 (0 to 1.2 V), the current rises to the plateau region at > 0.40 V and reaches the plateau at +0.60 V. On the reverse scan (1.2 to 0 V), the fall from the plateau occurs almost immediately and is very sharp below +0.9 V. The current reaches a minimum at +0.5 V and then increases until it meets the original forward scan (at +0.4 V) which it then follows back to the starting point (0 V SCE). Since at potentials of the order of 0.4 V (SCE) no oxide is present on a Pt surface,[6] we can thus conclude that on the reverse scan the oxidation of Fe^{2+} is inhibited by Pt-O formed at high potentials and that the original behavior of an oxide free surface is again restored at lower potentials, as is, in fact, indicated by the current increase at +0.5 V.

Thus it would appear that a slowly reduced oxide is formed on a C-anode at > +1.2 V (SCE) which inhibits the oxidation of Fe^{2+} to Fe^{3+}. This inhibition of the reaction is reflected by a shift in the diffusion limited plateau for the reaction to more positive potentials. Provided the electrode is not cycled beyond +1.2 V, no such inhibition occurs. Holding the electrode at -0.8 V will reduce this oxide.

Having established that the limits of the electrode were satisfactory, a series of E versus i curves was measured in solutions containing varying Fe^{2+} concentrations. Typical data in 10^{-3}M Fe are shown in Fig. 7 at varying rotation speeds. Clearly, the current is insignificant to +0.30 V (SCE), when a sharp rise to a plateau is observed [the latter is attained close to +0.50 V (SCE) and extends to +1.30 V (SCE), when O_2 evolution then sets in]. The slightly sloping character of the plateau is probably a reflection of the increase in background current as the voltage is made more positive. Clearly, the plateau current increases with increase in rotation speed, as would be expected from a purely mass transport limited process.

The above results, and others at varying Fe^{2+} concentration (10^{-2} to 5×10^{-4}M) are plotted as plateau current (corrected for background) versus

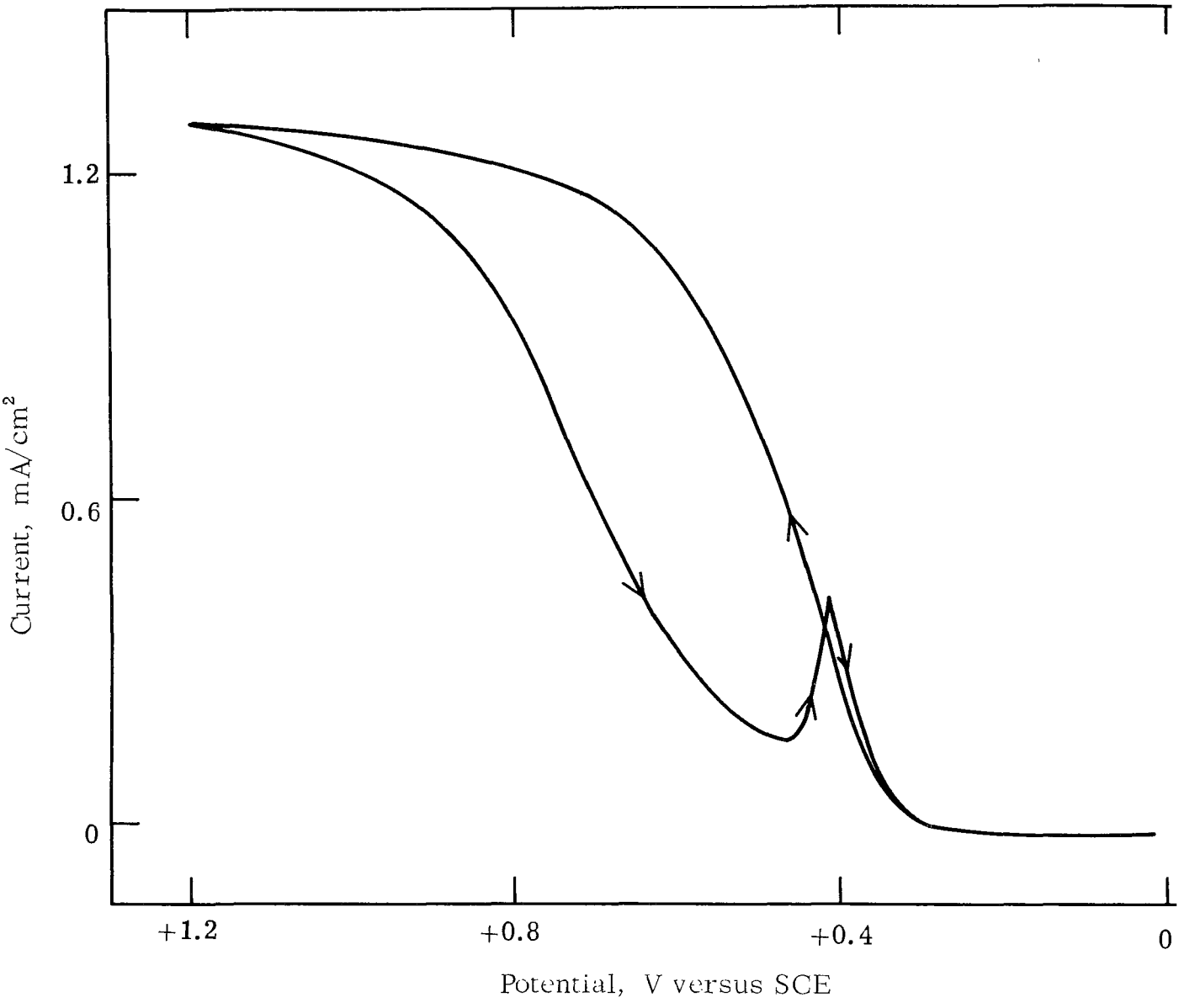

Fig. 6. Typical current-voltage scan to 1.2 V (SCE) on a platinum electrode in 0.02M H_2SO_4 containing 0.01M Fe^{2+} (scan rate = 0.10 V/min, rotation speed = 23.4 rps)

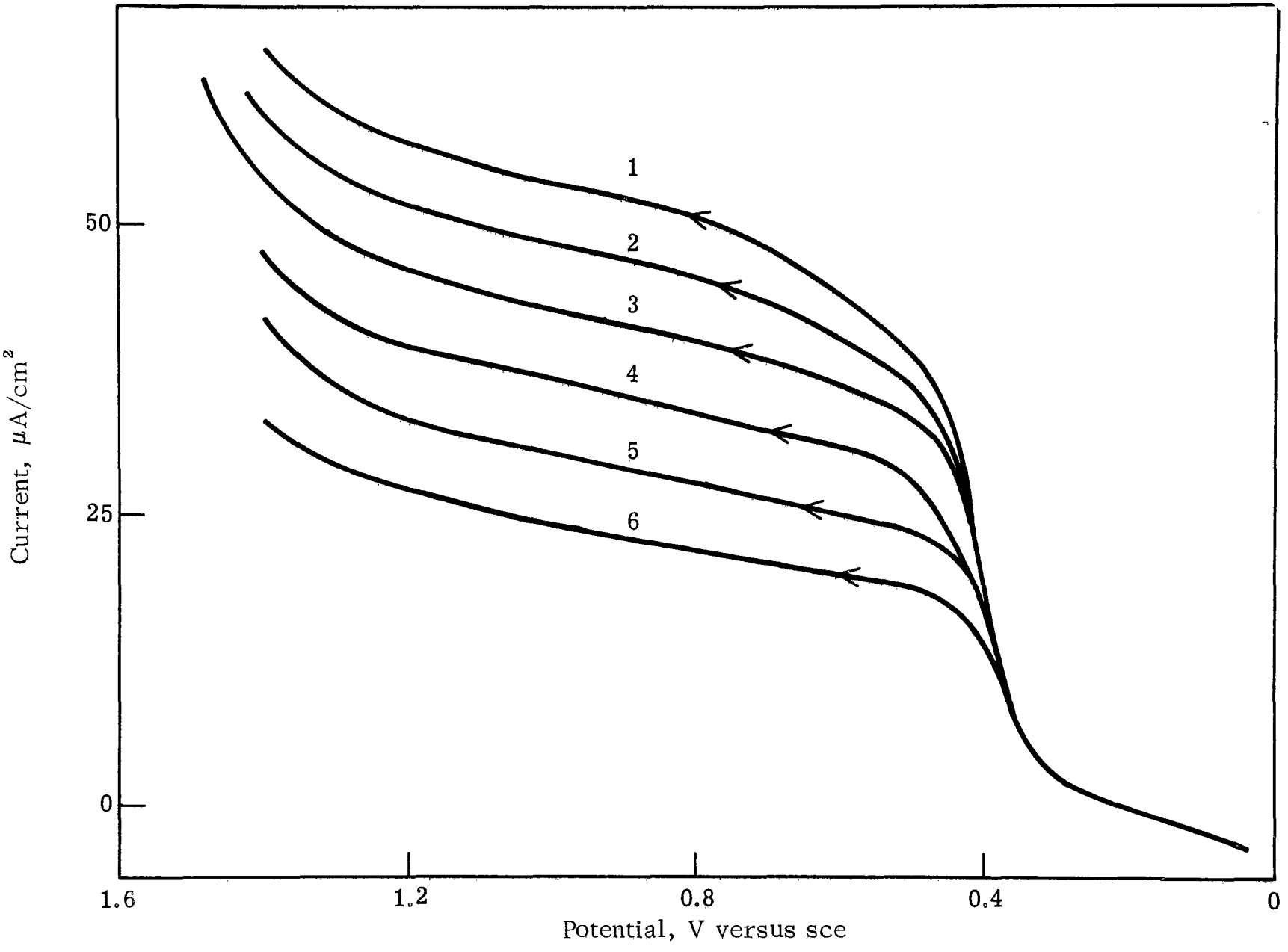

Fig. 7. Typical current-voltage scans on a vitreous carbon electrode in 0.02M H_2SO_4 containing 10^{-3}M Fe^{2+} (scan rate = 0.10 V/min)

$(\omega)^{1/2}$. As may be seen from Fig. 8 in every case a linear relationship is obtained, with the extrapolated current passing through the origin. This is exactly what would be expected for a purely mass transport limited process. Moreover, assuming a diffusion coefficient for Fe^{2+} of 5×10^{-6} cm^2/sec and a value for the kinematic viscosity of 2.15 $(\upsilon^{-1/6})$ $cp/cm^3/g$ (this is the value for 1M H_2SO_4,[9] and is probably slightly high), then, in 10^{-2}M Fe^{2+} solution, a diffusion limited current of 252 μA would be expected at a rotation speed of 13.5 rps, assuming a one-electron transfer process [Eq. (2)]. The measured value was 230 μA. We conclude from the above results that the plateaus shown correspond to the mass transport limited oxidation of Fe^{2+} to Fe^{3+}.

The oxidation of Fe^{2+} was examined in solutions which varied in both Fe^{2+} content and also Fe^{3+} content. Rotation speed of the electrode was varied and the oxidation currents were recorded at +1.2 V (SCE). These currents, corrected for background are shown in Fig. 9 for various ratios of Fe^{3+}/Fe^{2+}. In all cases, the oxidation currents were directly proportional to the square root of electrode rotation speed. Calculated values are shown on the graph also for each Fe^{2+} concentration and they agree very well with experimental values. As the figure shows, the presence of Fe^{3+} in solution does not affect the kinetics of oxidation process.

The reversible potential for the redox couple Fe^{3+}/Fe^{2+} can be calculated directly from the Nernst equation,[7] thus:

$$E_{redox} = E_0 + \frac{RT}{nF} \ln \frac{a_{Fe^{3+}}}{a_{Fe^{2+}}} \qquad (9)$$

where:

E_0 = standard equilibrium potential of the Fe^{3+}/Fe^{2+} couple

n = number of electrons involved in the reaction (= 1 here)

$a_{Fe^{3+}}/a_{Fe^{2+}}$ = ratio of the activities of the oxidized and reduced species in the reaction (we have taken concentrations only here)

It is clear from this equation that the redox potential will change in proportion to any change in activity ratios. This is shown graphically in Fig. 10. As the ratio Fe^{3+}/Fe^{2+} increases, the redox potential shifts more positive. For example, when the Fe^{3+}/Fe^{2+} ratio in solution is increased from 10^{-2} to 10 the reversible potential of the changes from approximately +0.41 to +0.57 V (SCE). This is, for present purposes, a negligible change.

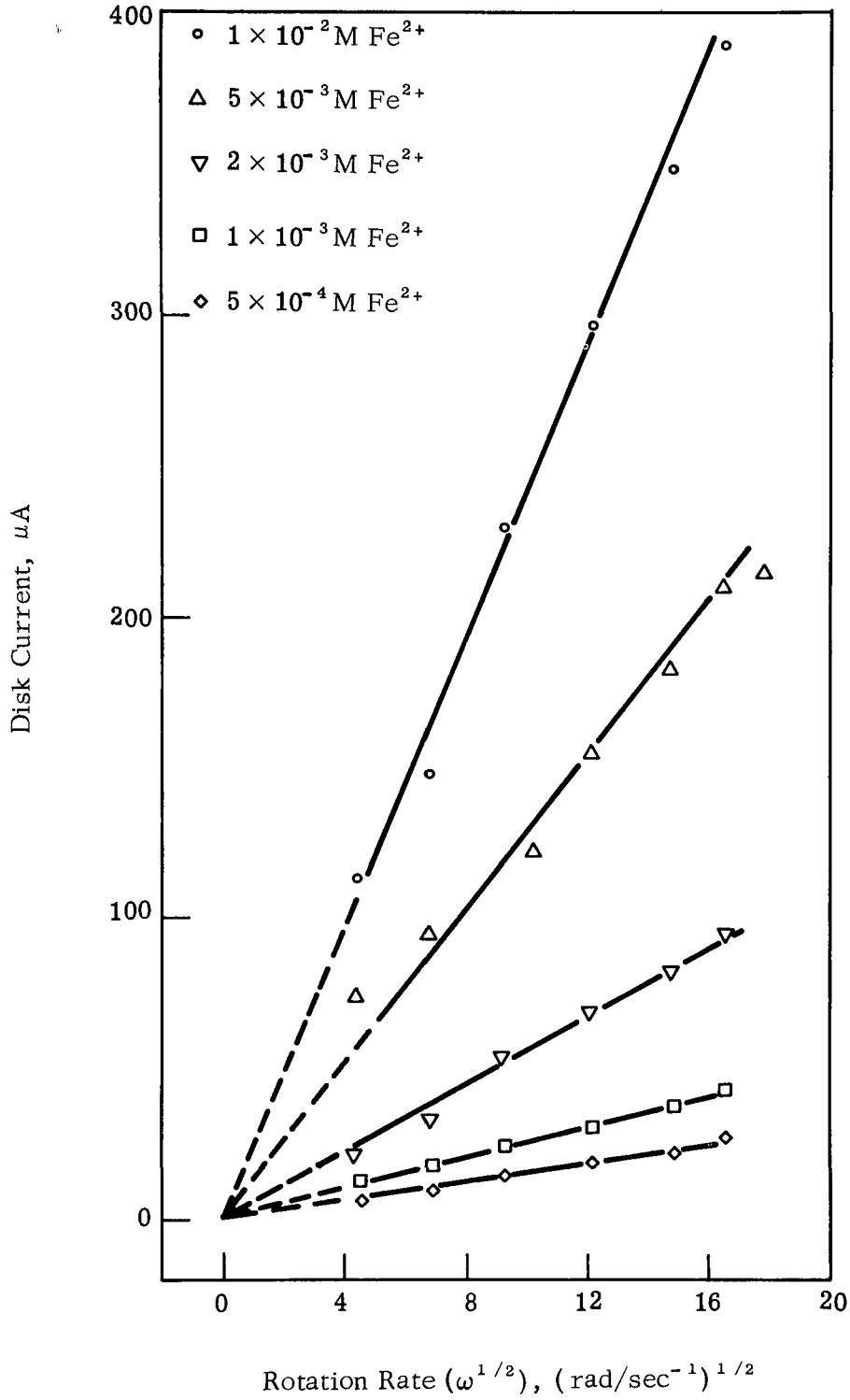

Fig. 8. Relation between electrode rotation speed and plateau currents during the oxidation of Fe^{2+} to Fe^{3+} in 0.02M H_2SO_4 containing a range of Fe^{2+} concentrations

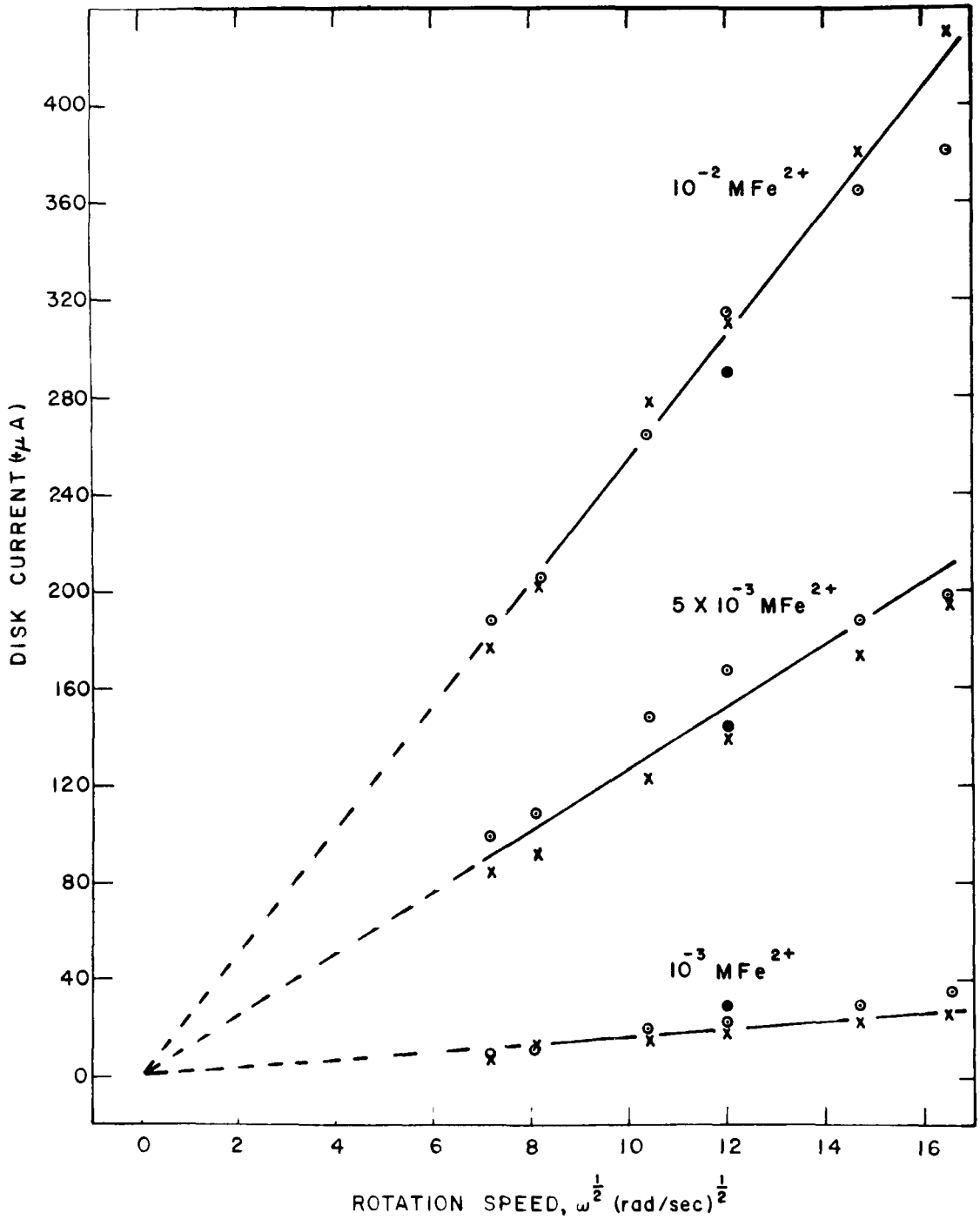

Fig. 9. Oxidation of Fe^{2+} to Fe^{3+} at a rotating carbon anode in 0.02M H_2SO_4 containing varying amounts of Fe^{3+} and Fe^{2+} species (x, 10^{-2}M Fe^{3+}; ⊙, 10^{-3}M Fe^{3+}; ●, Calculated Currents)

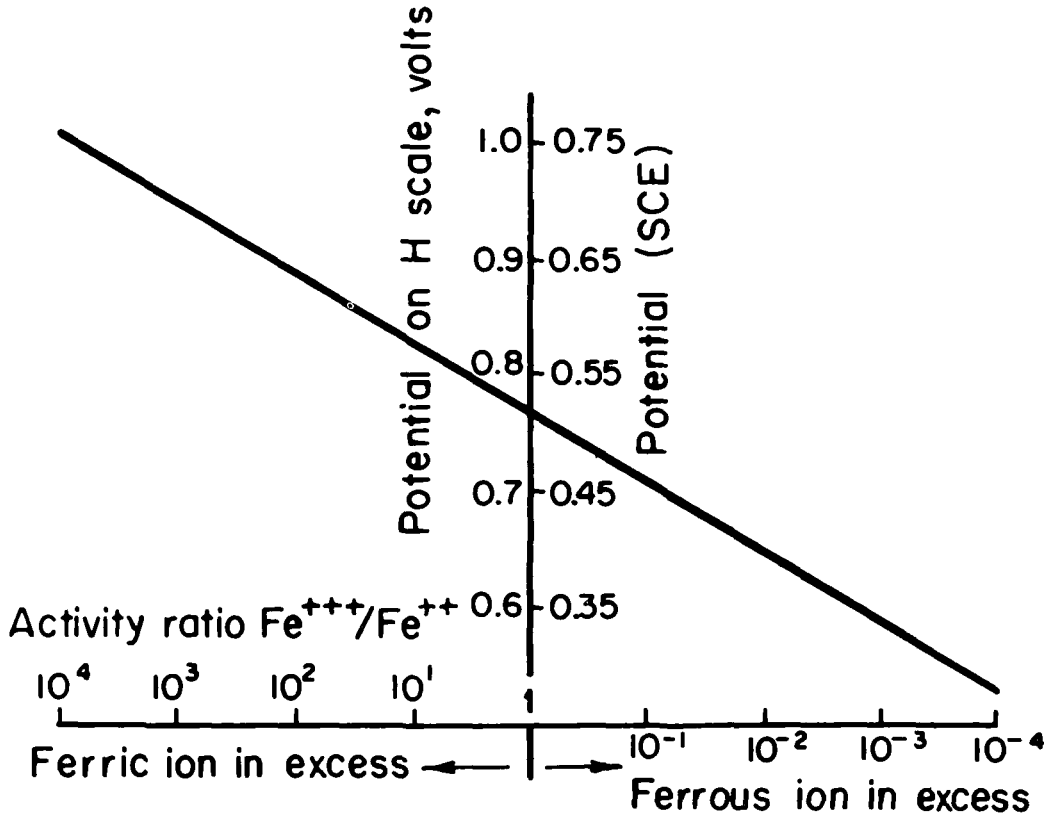

Fig. 10. Reversible potential of the Fe^{3+}/Fe^{2+} system on platinum at 25 °C

It can be shown[7] that the equation expressing the relationship between current, electrode potential and ion concentration also involves the log term of Eq. (9). In the present experiment, it was difficult to evaluate changes in potential over a wide range of Fe^{3+}/Fe^{2+} ratios since the oxidation current for Fe^{2+} becomes quite small at $< 10^{-3}$M Fe^{2+} concentrations, even at the highest electrode rotation speed. However, a 130 mV negative shift was observed in the plateau potential for the data in Fig. 9 as the Fe^{3+}/Fe^{2+} ratio was varied from 1/1 to 1/10.

The above is illustrated more clearly in Fig. 11 where are shown two current-voltage curves on a carbon electrode in 0.02M H_2SO_4 containing approximately 5×10^{-4}M Fe^{2+} and 5×10^{-4}M $Fe^{2+} + 5 \times 10^{-2}$M Fe^{3+}, respectively. The activity (concentration here) ratio varies from an overwhelming excess of Fe^{2+} (i.e., no Fe^{3+} added) to a 100/1 excess of Fe^{3+}. Data were obtained on a freshly polished electrode which was held at -0.90 V for 5 min initially to reduce any oxide present. The first scan after this procedure was not well defined and current flow commenced at +0.50 V reaching a plateau at +1.0 V. Thereafter, the electrode was scanned from +0.20 to +1.40 V and only a slight shift in the curves towards more negative potentials was observed on each succeeding scan. Scan A in Fig. 11 is a typical one for a concentration of 6.7×10^{-2}M Fe^{2+}. The current is substantially zero to near +0.35 V when a sharp increase is observed to a "sloping plateau" at +0.50 V, which continues to +1.40 V. Curve B in Fig.11 illustrates the effect on the curve of added Fe^{3+} (5.43×10^{-2}M). The Fe^{2+} content here was 5.50×10^{-4}M. The current is negative until +0.55 V when a sharp increase is observed to a plateau at +0.65 V, which continues to +1.40 V. That is, a 0.150 V shift to more positive potentials is observed by adjusting the Fe^{3+}/Fe^{2+} ratio from no Fe^{3+} content to a 100/1 excess of Fe^{3+}. The diffusion currents for Fe^{2+} oxidation can be calculated in both cases. Hence, in 6.7×10^{-4}M Fe^{2+} solution at a rotation speed of 23 rps, a limiting current of 20.5 μA would be expected, compared to 15.2 μA in 5.5×10^{-4}M Fe^{2+} solution at the same electrode rotation speed. At +1.2 V, the observed values, corrected for background, are 26 μA and 15 μA, respectively. It is thus clear that Fe^{3+} in solution does not affect Fe^{2+} oxidation even at high excess of Fe^{3+} and there is a workable potential region to use for Fe^{2+} oxidation even when the Fe^{3+}/Fe^{2+} ratio in solution changes considerably

CATHODIC PROCESSES

H_2 Evolution: The described cathodic process is the reduction of hydrogen ion to hydrogen gas, i.e.,

$$2H^+ + 2e^- \rightarrow H_2$$

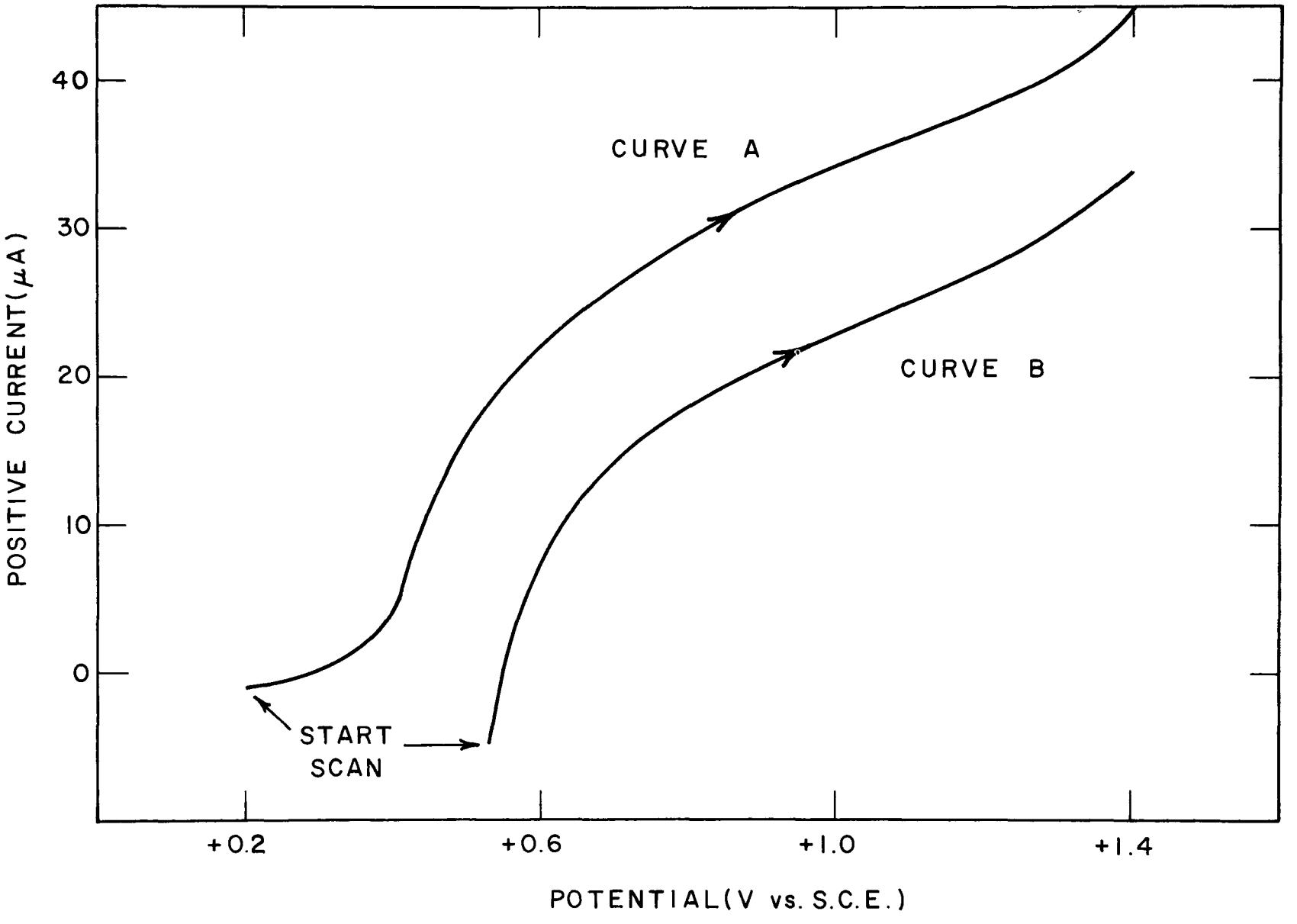

Fig. 11. The effect of varying the Fe^{3+}/Fe^{2+} ratio in solution on the current potential curve for Fe^{2+} oxidation at a carbon anode in 0.02M H_2SO_4 (Curve A, no Fe^{3+} present; Curve B, 100/1 Fe^{3+}/Fe^{2+} Ratio)

The current-potential dependence for this reaction traditionally has involved a pronounced dependance on the chemical composition of the electrode surface. For nonelectrochemical reasons, 316-stainless steel was chosen as the anode material. It remained to be determined whether this decision was indeed a workable one. As a first step, the formation and reduction of surface oxides were studied on the 316-stainless steel cathode in 0.02M H_2SO_4.

On freshly polished stainless steel, an open circuit potential (E_{OC}) was observed in deaerated solution in the region of +0.110 V (SCE). A typical current-voltage scan at 0.03 V/min is shown in Fig. 12. The current is very small (< 5 μA) from E_{OC} to +0.80 V (SCE); above this, a sharp increase in current with increase in potential is observed which reaches a maximum typically in the region of +350 μA, at 1.1 V (SCE). At more positive potentials, the current decreases slightly to a minimum before rising sharply again at 0.04 V (O_2 evolution).

The reverse scan on the electrode to more negative potentials follows the forward one closely and the current is insignificant to -0.40 V. Below this potential, the current then increases rapidly to about 1 mA at -0.80 V. When the scan is again reversed, some hysteresis in these high currents is observed as evidenced by a 0.004 V shift in the return scan to more noble potentials.

The above experiment on this electrode was repeated several times, each time scanning to more negative potentials. The most striking differences in the curves so obtained are that the H_2 currents on the electrode (< -0.40 V) during the forward and reverse scans show greater hysteresis as the reverse scans are carried out to more negative potentials. Secondly, an anodic peak appears at -0.040 V when the scan is first made to < -0.80 V, and it increases in size as the scans are carried out to more negative potentials.

The obvious explanation for these results is that, when the stainless steel is first immersed in the 0.02M H_2SO_4, it spontaneously passivates, i.e., the observed E_{OC} of +0.11 V is actually within the passive region for the alloy in these environments. Riggs[8] shows polarization curves for 316-stainless steel in 10M H_2SO_4 in which the active to passive transition occurs over the range -0.40 to 0.0 V (SCE). This spontaneous passivation does not occur in 1M H_2SO_4 where the observed E_{OC} is -0.350 V. When the electrode is passivated in the latter environment, the active to passive transition is observed in the active to noble (positive) potentials scan but not in the reverse direction. This is obviously what happens also in 0.02M H_2SO_4 and indicates that the Fe_2O_3, Cr_2O_3 passivating film is difficult to reduce on the surface once it is formed. The results do indeed show that quite negative potentials (< -0.80 V) have to be reached before significant reduction of the passivating film occurs.

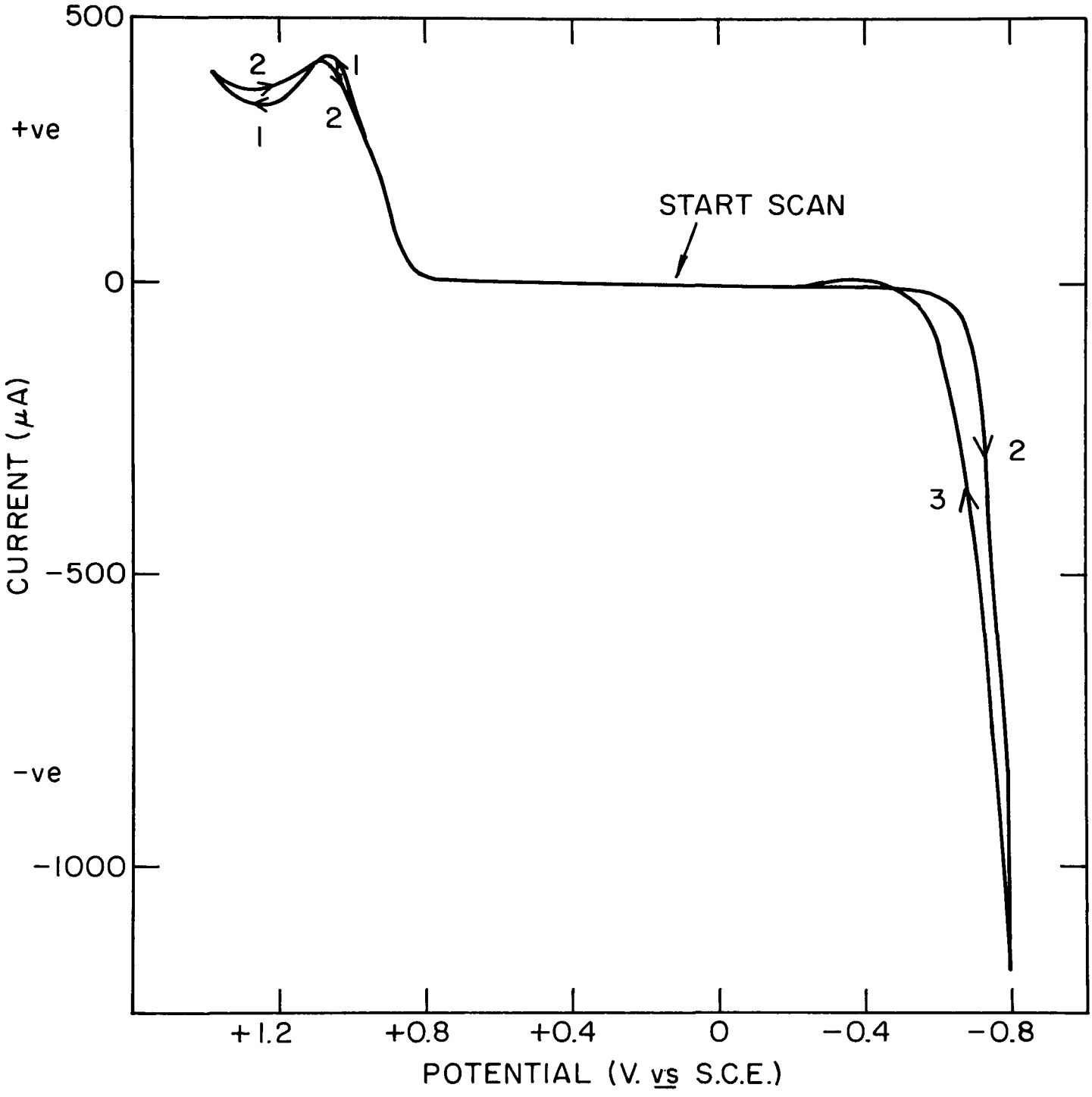

Fig. 12. First voltage scan to -0.80 V freshly polished on a 316 stainless steel cathode in deaerated 0.02M H_2SO_4 at ambient temperature (scan rate = 0.102 V/min)

The slight peak observed at $> +0.80$ V (in the transpassive region) is most likely due to some gross and relatively porous oxide layer (or hydroxide or sulfate) on the surface. In any event, corrosion of the surface protective oxides occurs readily here and no protective ability is obtained. Secondly, and more important, stainless steel in 0.02M H_2SO_4 environments is effectively anodically protected and will thus corrode only at an infinitesimal rate ($< 0.5\ \mu A/cm^2$).

The divergence of the H_2 curves on the two scans can be explained by the presence of the oxide film. Obviously the H_2 currents at equivalent potentials are greater on the "bare" surface than on the oxide coated one, as would perhaps be expected.

In order to evaluate this point, the electrode was potentiostatted at -1.0 V for 10 min to remove any surface oxides on the steel. Once we had carried out this reduction step, the electrode was held sufficiently negative so that the oxides were not again formed on the surface. The current-potential behavior was then measured by potentiostatting the electrode in multiples of 0.05 V steps negative of the start of the Tafel region [generally -0.50 V (SCE)]. After 1 min when the currents were generally steady, the electrode was returned to the start of the Tafel region and left for 5 min. After this, the procedure was repeated and the current measured at the next potential value.

In Fig. 13, we show a comparison in the E versus i curves obtained in 0.02M H_2SO_4 on a stainless steel surface passivated (with oxide) and oxide free. The Tafel slope on the oxide free surface (138 mV/decade) is greater than on the passivated surface (100 mV/decade). At a given value of potential, currents on the oxide free surface are greater than on the passivated surface. For example, at -0.50 V, the relative values are 37.0×10^{-6} A/cm^2 and 4.5×10^{-6} A/cm^2, respectively. At < -0.75 V, the curves converge. This is as expected since the oxide on the passivated surface will be reduced in this potential region.

There is a tendency for the E versus i curves to flatten out to a plateau region at < -0.70 V. To determine if this represented the onset of mass transport limited H_2 evolution on the electrode, the following experiments were carried out. At a rotation speed of 4.1 rps and assuming $D^{H+} = 7.45 \times 10^{-5}$ cm^2/sec[10] in 0.01M H_2SO_4 solution, a diffusion current for H^+ to the disk of 11.7 mA/cm^2 was calculated. The measured value at < -1.0 V was 13 mA/cm^2. What was puzzling however was that, at the higher rotation speeds examined (up to 51.6 rps), the currents did increase slightly but not in the calculated manner. Indeed at 23.8 rps and 51.6 rps, the current in the plateau region for H_2 evolution was constant. Also, no well defined plateau was observed

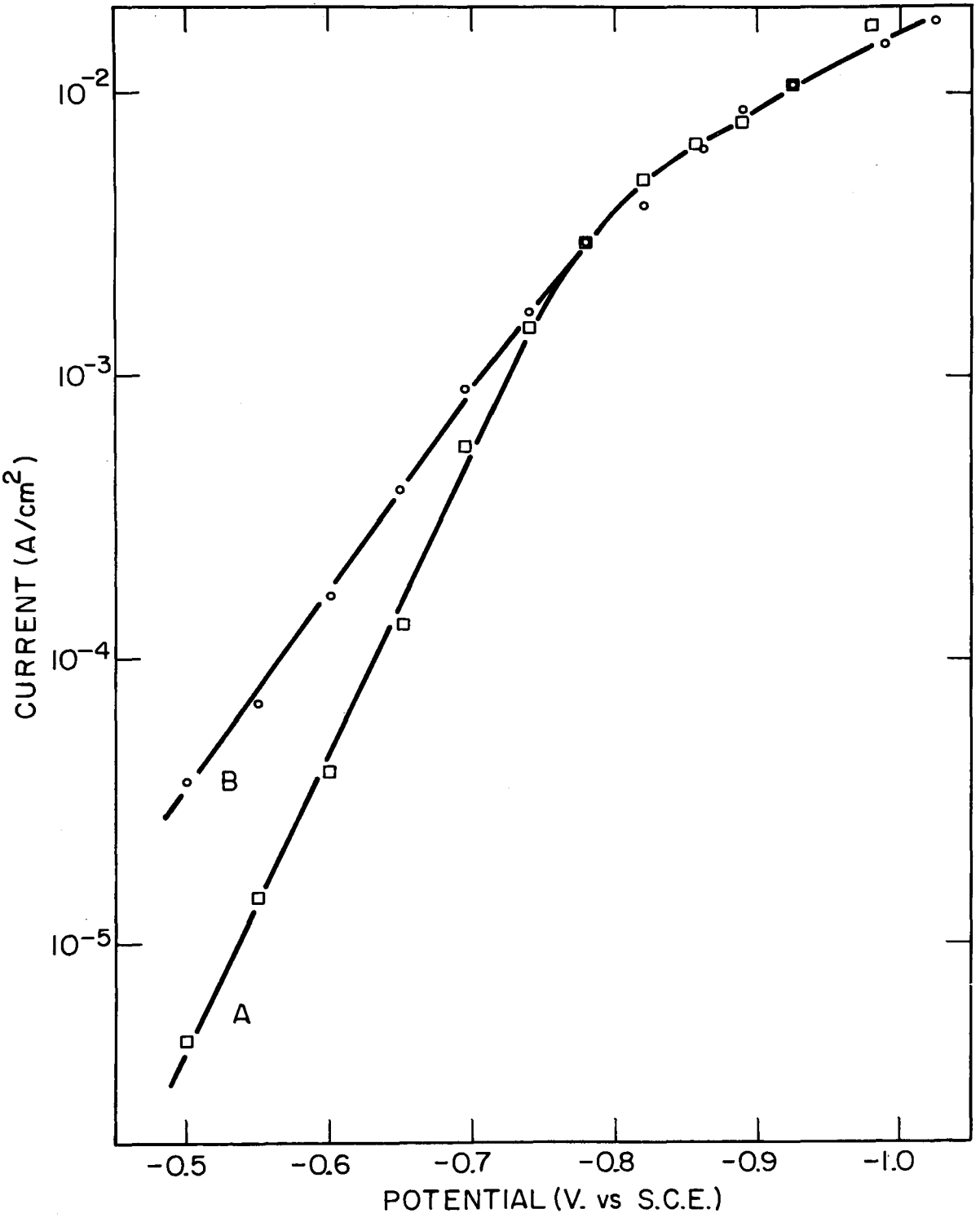

Fig. 13. Hydrogen evolution characteristics on a passivated (A) and oxide free (B) 316 stainless steel surface in 0.02M H_2SO_4 at ambient temperature

but instead the current increased from 14.0 mA/cm^2 at -1.2 V to 62 mA/cm^2 at -2.5 V. In line with mass transport limitations, currents were greater in 0.02M H_2SO_4 solution.

These data were repeated in the same solutions and in 10^{-3}M H_2SO_4. The results, summarized in Fig. 14, show exactly the same trend. Deviations from the Tafel regions occur at less negative potentials and the "sloping" plateaus are reached at lower current levels as the acid concentration is reduced. In these plateaus, currents tend to be independent of rotation speed of the electrode. The most likely explanation for the data is that mass transport is not limiting but rather that an adsorption step or electrochemical discharge step limits the overall rate of the reaction.

Back Reduction of Fe^{3+}: An obvious complication in the total process for Fe^{2+} oxidation is that Fe^{3+} produced at the carbon anode may be swept over to the steel cathode and reduced back to Fe^{2+} or indeed to Fe. Already shown were the potentials where significant H_2 currents can be attained on a steel cathode. Additional information is also required on where (i.e., at what potentials) significant reduction of Fe species can take place also on this cathode. If these two regions overlap, then it may be necessary to shield the cathode from Fe^{3+} oxidized at the anode by using some type of membrane.

A preliminary scan on a rotating steel electrode to determine where Fe^{3+} is reduced to Fe^{2+} and Fe is shown in Fig. 15. Data were obtained in 2×10^{-3}M Fe^{3+} solutions in 0.02M H_2SO_4 at a scan rate of 0.102 V/min and a rotation speed of 51.1 rps. On the forward scan (+0.20 V to -0.70 V), the current does not increase significantly until -0.20 V when a rise to a small plateau is observed near -0.60 V. Above this, currents increase sharply. Reversal of the scan at this point leads to a well defined plateau from -0.60 V to -0.20 V which then falls sharply between -0.20 V and 0 V. The current in this plateau region is 716.7 μA. Assuming a diffusion coefficient for Fe^{3+} of 2×10^{-6} cm^2/sec[11] and taking a rotation speed of 51.1 rps, then from the limiting diffusion equation to a rotating disk, a current of 758 μA would be expected from a one-electron transfer process namely, $Fe^{3+} + e^- \rightarrow Fe^{2+}$. We attribute the plateau in Fig. 15 to this reaction then.

The data on Fig. 16 illustrate the sixth scan on an electrode which had also been left at +0.140 V for 1 hr before the scan and indicate widely different current voltage characteristics. Here reverse and forward scans are much closer together and show no plateaus. In addition, the current levels are smaller than in Fig. 15. Thus, the currents at -0.60 V are 340 μA on forward and reverse scans respectively, compared to 420 μA for the first scan on the electrode (Fig. 15).

The explanation for these observations lies simply in the fact that the protective oxide coating is also formed on the electrode here [the E_{OC} is +0.200 V

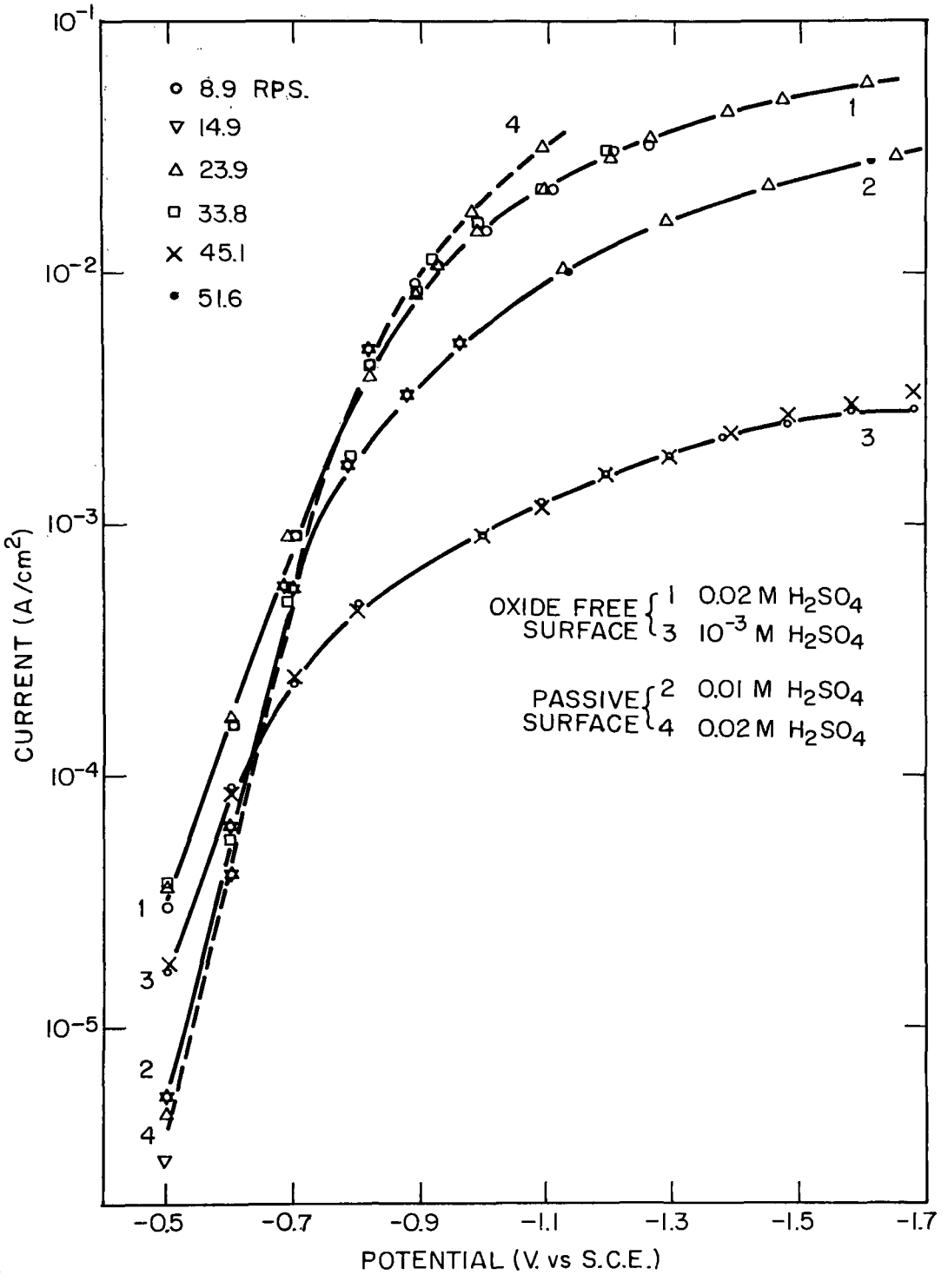

Fig. 14. The effect of H_2SO_4 concentration and electrode rotation speed on the hydrogen evolution reaction on a 316 stainless steel surface at ambient temperature

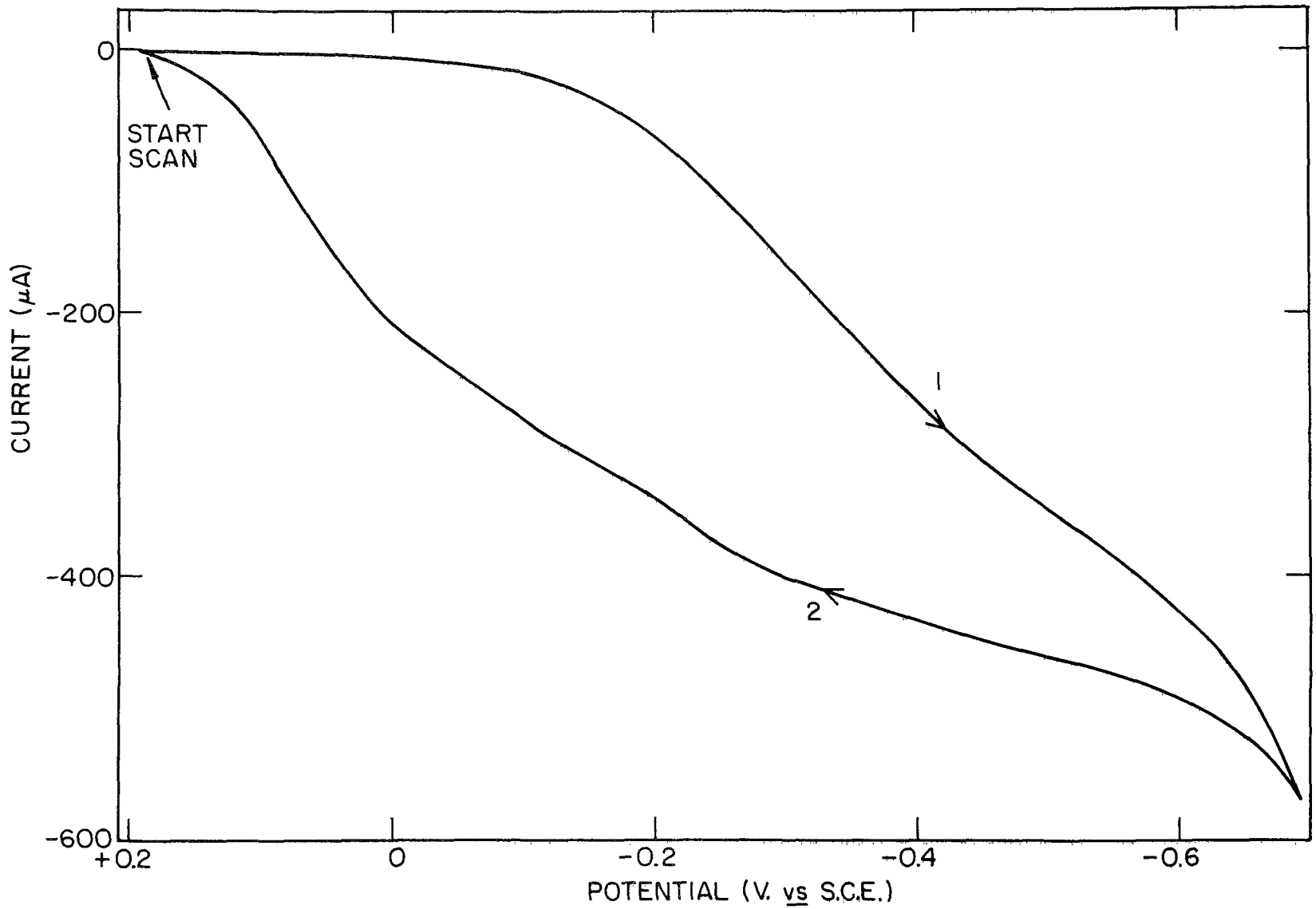

Fig. 15. First voltage scan to -0.70 V on a freshly polished 316 stainless steel cathode in deaerated 0.02M H_2SO_4 solution at ambient temperature and containing 2×10^{-3}M Fe^{3+} (scan rate = 0.102 V/min)

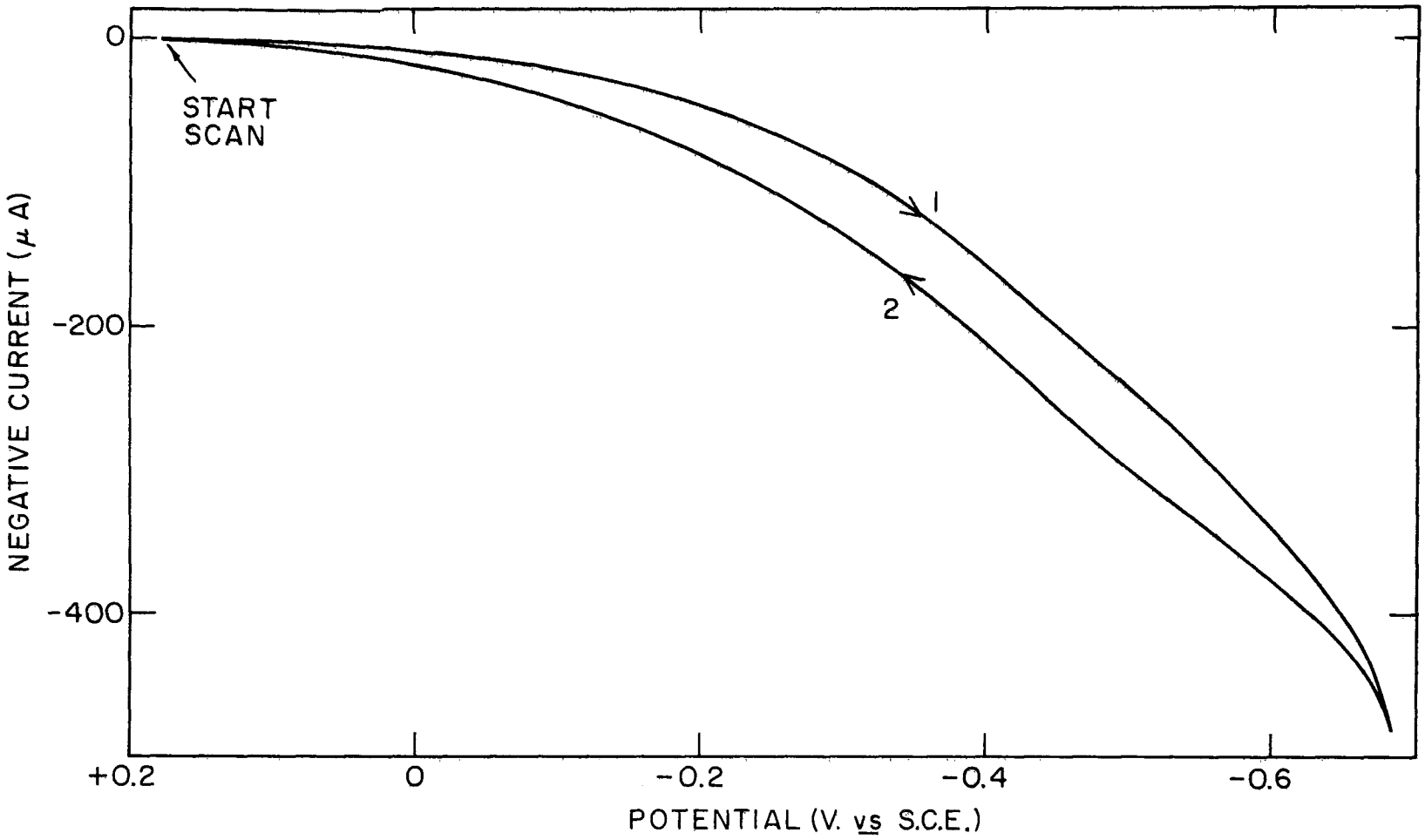

Fig. 16. Sixth voltage scan to -0.70 V on a freshly polished 316 stainless steel cathode in deaerated 0.02M H_2SO_4 solution at ambient temperature and containing 2×10^{-3}M Fe^{3+} (scan rate = 0.102 V/min)

(SCE) in Fe^{3+} solutions] and is not removed by scanning to -0.70 V. As the number of scans between +0.20 and -0.70 V is increased and the time of immersion of the electrode at positive potentials is increased ($\leq$ +0.20 V), the protective oxide film is thickened and thus its inhibiting effect on the $Fe^{3+} \rightarrow Fe^{2+}$ reduction process becomes more pronounced.

To confirm these conclusions, the electrode was scanned more negative and the effect of this on the $Fe^{3+} \rightarrow Fe^{2+}$ reduction plateau was monitored. It was found necessary to scan to between -0.80 and -0.90 V before a well defined plateau was observed on the reverse scan to more noble potentials. In all cases, when the electrode was brought to +0.20 V before each scan, a hysteresis was observed between the forward and reverse scans at $>$ -0.30 V and amounting to $\sim$ 0.150 V. The scans on the two plateaus coincided at $<$ -0.30 V. This is shown clearly in Fig. 17 where the negative scan was to -0.90 V. It is interesting to note that a slight dip occurs at -0.225 V in plateau obtained during the reverse scan on the electrode. This could be due to a superimposed oxidation of Fe (to Fe^{2+}) plated onto the electrode at -0.90 V but, more likely, it is caused by anodic oxide formation on the electrode. In any event, it seems that oxide at this stage is not quite so inhibiting on the Fe^{3+} reduction process since the plateau is again observed at -0.20 V before it drops off to zero current between -0.150 and +0.20 V. Obviously also, once all the Fe^{2+} is oxidized off the surface (at +0.20 V), the inhibiting effects of the oxide film again came into play. It is worth noting finally that, if the negative scan is only carried out to -0.80 V, then the fall in current in the reverse plateau occurs between -0.20 and 0.9 V. Also, the dip in this plateau at -0.225 V is not observed here. Both facts provide further evidence of the stability of the protective oxide at negative potentials and of its effect on the reduction process when it is present on the surface in the absence of Fe^{2+}. In line with earlier data in 0.02M H_2SO_4 only (i.e., no Fe^{3+} present), these results show that the oxide is not substantially reduced at until $\leq$ -0.90V. This is also why the reduction plateau for $Fe^{3+} \rightarrow Fe^{2+}$ (-0.150 to -0.60 V) is not observed until potentials are more negative than would be expected from the literature value of +0.340 V (SCE)[3] (10^{-3}M Fe^{3+} solution).

Having clarified the processes operative on the stainless steel electrode in these environments, a final check was required that the plateau between $\sim$ 0 and -0.60 V on the oxide-free electrode was indeed due to the reduction of Fe^{3+} to Fe^{2+} at a diffusion limited rate. The Fe^{3+} concentration in 0.02M H_2SO_4 was thus varied from 2×10^{-4}M to 3.7×10^{-3}M and cyclic scan experiments were run on the electrode at various rotation speeds for each concentration. In all cases, the electrode was scanned to -1.0 V (the current here was generally 5.9 mA) before measuring the current on the reverse plateau (oxide-free electrode). The data are a linear function of rotation speed as would be expected from a diffusion limited process on a rotating disk electrode. Also, the current at a given rotation speed is directly proportional to Fe^{3+} concentration. For example, at $\omega^{1/2}$ (rotation speed)$^{1/2}$

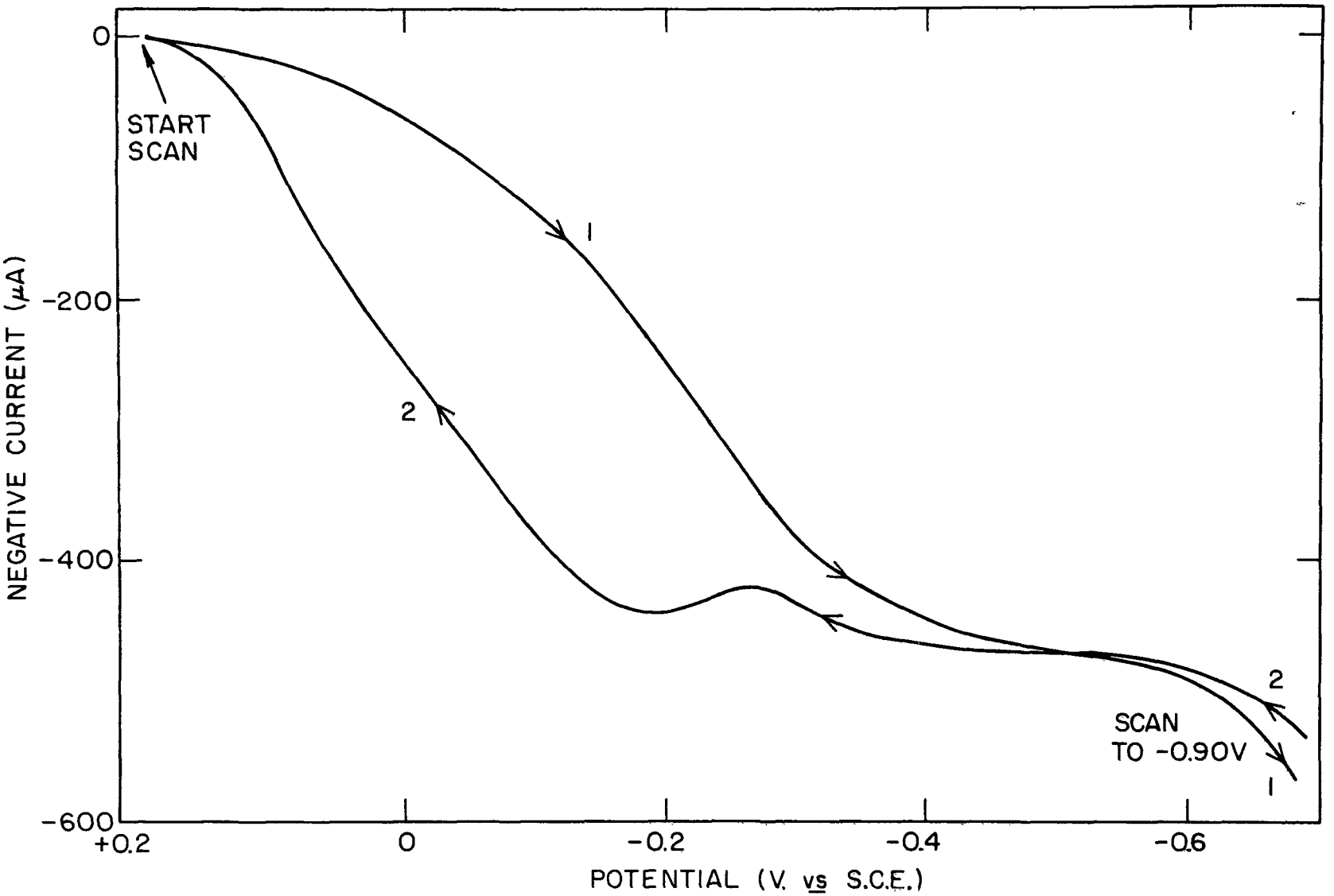

Fig. 17. Voltage scan to -0.90 V on a stainless steel cathode in deaerated 0.02M H_2SO_4 solution at ambient temperature and containing 2×10^{-3}M Fe^{3+} (scan rate = 0.102 V/min)

equal to 14 rad/sec$^{1/2}$, the current in 2×10^{-4}M Fe^{3+} is 42.5 μA; it is 470 μA in 2×10^{-3}M Fe^{3+}; and it is 990 μA in 3.7×10^{-3}M Fe^{3+}. Based on the latter current and concentration, currents of 535 μA in 2×10^{-3}M Fe^{3+} and 53.5 μA in 2×10^{-4}M Fe^{3+} solutions would be expected.

The diffusion limited current to a rotating disk electrode can readily be calculated. At $\omega^{1/2}$ equal to 14 rad/sec$^{1/2}$, we would expect current of 874.9 μA, 472.9 μA in 3.7×10^{-3}M Fe^{3+}, 2×10^{-3}M Fe^{3+}, and 2×10^{-4}M Fe^{3+} solutions for a one-electron reduction process to Fe^{2+}. The observed values are 990, 470, and 42.5 μA, repsectively, in these concentrations. The agreement is thus good and indicates that the reduction plateau on the "oxide free" stainless steel electrode from -0.150 to -0.60 V is due to diffusion limited reduction of Fe^{3+} to Fe^{2+} species.

Deposition of Metallic Iron: It has been demonstrated that reaction ($Fe^{3+} \rightarrow Fe^{2+}$) occurs over the range -0.15 to -0.60 V at a diffusion limited rate prior to onset of H_2 evolution. In the next experiments, the cathode was scanned generally between 0.0 and -1.0 V in an attempt to isolate a diffusion limited plateau for Fe^{3+} reduction to the metal. Electrode rotation speed was varied. In 2×10^{-3}M Fe^{3+} at 23.4 rps, assuming a diffusion coefficient for Fe^{3+} of 4.1×10^{-6} cm^2/sec,[11] a diffusion limited current of 1.23 mA for reduction to the metal would be expected. In some scans, a slight plateau was observed at $<$ -0.80 V. This was not, however, reproducible though it occurred generally at current levels of 0.90 to 1.4 mA. It was not strikingly dependent on rotation speed. It was therefore not possible to conclude with any degree of certainty whether or not Fe^{3+} is reduced to the metal at $<$ -0.60 V on a stainless steel cathode. Essentially H_2 evolution on the cathode interferes with a detailed examination of this potential region.

The next experiments used a cylindrical 316 stainless steel electrode of area 3.6 cm^2 which was potentiostatted for 90 hr at -1.0 V (SCE) in 0.02M H_2SO_4 containing 4×10^{-2}M Fe^{3+} The electrode was brightly polished beforehand and was also weighed. At -1.0 V, a constant current of 23 mA was recorded. The diffusion limited current of a dissolved electroactive species to a stationary electrode is given by the equation:[5]

$$i = \frac{nFDCA}{\delta} \qquad (10)$$

where:

C = concentration of moles/cc

A = area of the electrode (cm^2)

δ = thickness of the diffusion layer (normally 0.05 cm in unstirred solution)

Based on the equation, a current of 3.5 mA would be expected for reduction of Fe^{3+} to Fe in 4×10^{-2}M Fe^{3+} solution. Over a period of 90 hr, this would result in the deposition of 200 mg of Fe on the electrode. During the actual experiment, the entire electrode surface became dark and a weight increase of 11 mg was observed. Though this is significantly less than the calculated value, it can be inferred that reduction of Fe^{3+} (and Fe^{2+}) can occur on a 316 stainless steel cathode at potentials of the order of -1.0 V (SCE). Differences in calculated and observed weight change during deposition may be attributed to H_2 evolution in the same potential region interfering with Fe deposition and consequently with weight of Fe deposited. In a practical setup, it is evident that quite large currents (large overpotentials) can be supported on the cathode before Fe deposition takes place. Normally then, this will not be a problem.

TIME DEPENDENT PROCESSES

The experiments described to this point have been entirely short term. It is important to realize, when evaluating such data and when trying to reproduce these results, that superimposed on the phenomenon discussed, there will always be a slow deactivation of the electrode surface from the absorption of trace impurities. Examples of this deactivation are given below. Before proceeding to this information, it is important to realize that the effects observed are general ones, common to most heterogeneous processes involving solid surfaces, i.e., a small concentration of surface active material is sufficient to rapidly deactivate a smooth solid surface. The classical solution to this problem is to increase surface area. Porous fuel cell electrodes are longer lived than smooth electrodes; porous petrochemical catalysts are longer lived than smooth catalysts. Most impurities reach the solid surface by diffusion and consequently the geometric area of the electrode is the important parameter in this respect. With highly porous electrodes, these impurities build up at pore mouth, while the desired reaction takes place slightly within the pore on clean surface.

Since this is so, one can ask the question: Why use smooth electrodes at all? Data of the type required to unravel the various reaction mechanisms are easiest to interpret with smooth electrodes. In other words, an idealized smooth vitreous carbon electrode was deliberately chosen for these studies to simplify investigating the electrochemical mechanistic aspects of the processes. When used in the form of a rotating disk, mass transfer conditions to this electrode were then exactly characterized. Unfortunately,

the very feature of the electrode that makes this possible, i.e., its smoothness, renders it highly susceptible to poisoning. Fortunately the time available before the poisoning process sets in had been sufficient to permit the acquisition of meaningful data.

To this point, the discussion may appear to be an excuse for a possible insoluble problem. Considerable credibility is given to the surface area protection argument from the data in Section 5 of this document. It will be shown that no deactivation is observed for high surface area carbon electrodes exposed for days to identical solutions which deactivated smooth electrodes in hours.

Fig. 18 shows a prolonged current transient in chemical AMD water containing 10^{-2}M Fe^{2+} in 0.02M H_2SO_4. The calculated limiting current for the Fe^{2+} oxidation to Fe^{3+} is 300 μA. The initial experimental current at +1.2 V is 335 μA, slightly higher than expected. More important, however, is the observation that this current is not sustained for any length of time but begins to decay rapidly and continues to do so, reaching a plateau at 212 μA after 14 hr immersion. This corresponds to a decrease in current of 36.7% over this time period.

At this point, the electrode was "cleaned" by pulsing it to -0.90 V and leaving it there for 5 min. An initial current at +1.2 V was 384 μA which fell to 330 μA after 0.5 hr. Thereafter, the current decreased to a plateau at 260 μA after 14 hr. These data are also shown in Fig. 18. The decrease in current here from the initial value of 384 μA corresponds to a 32.3% fall. The final plateau current is 48 μA greater than in the first case.

Following a similar cleaning procedure, the electrode was then potentiostatted at +0.90 V for 67 hr. An initial current of 300 μA fell to 223 μA after 14 hr and then to 165 μA after 66 hr. After 14 hr the decrease was 25.7% and after 66 hr the current was 55.0% of the original value. Cleaning the electrode at negative potentials is apparently more effective than doing so at positive potentials.

Similar data were obtained in a solution of chemical AMD containing 5×10^{-2}M Fe^{2+} as well as 5×10^{-2}M Fe^{3+} in 0.02M H_2SO_4. At +1.2 V, the initial current was 1360 μA and this decreased to a plateau value of 940 μA after 14 hr, corresponding to a 30.9% fall. The calculated current for Fe^{2+} oxidation in this solution is 1500 μA which is slightly larger than the experimental value. The current rose to 1250 μA at this point after the electrode was "cleaned" for 3 min at -0.9 V.

Clearly then, on the smooth electrode, even in pure chemical AMD solutions, there is a fall in Fe^{2+} oxidation current with time, which, in the worst case,

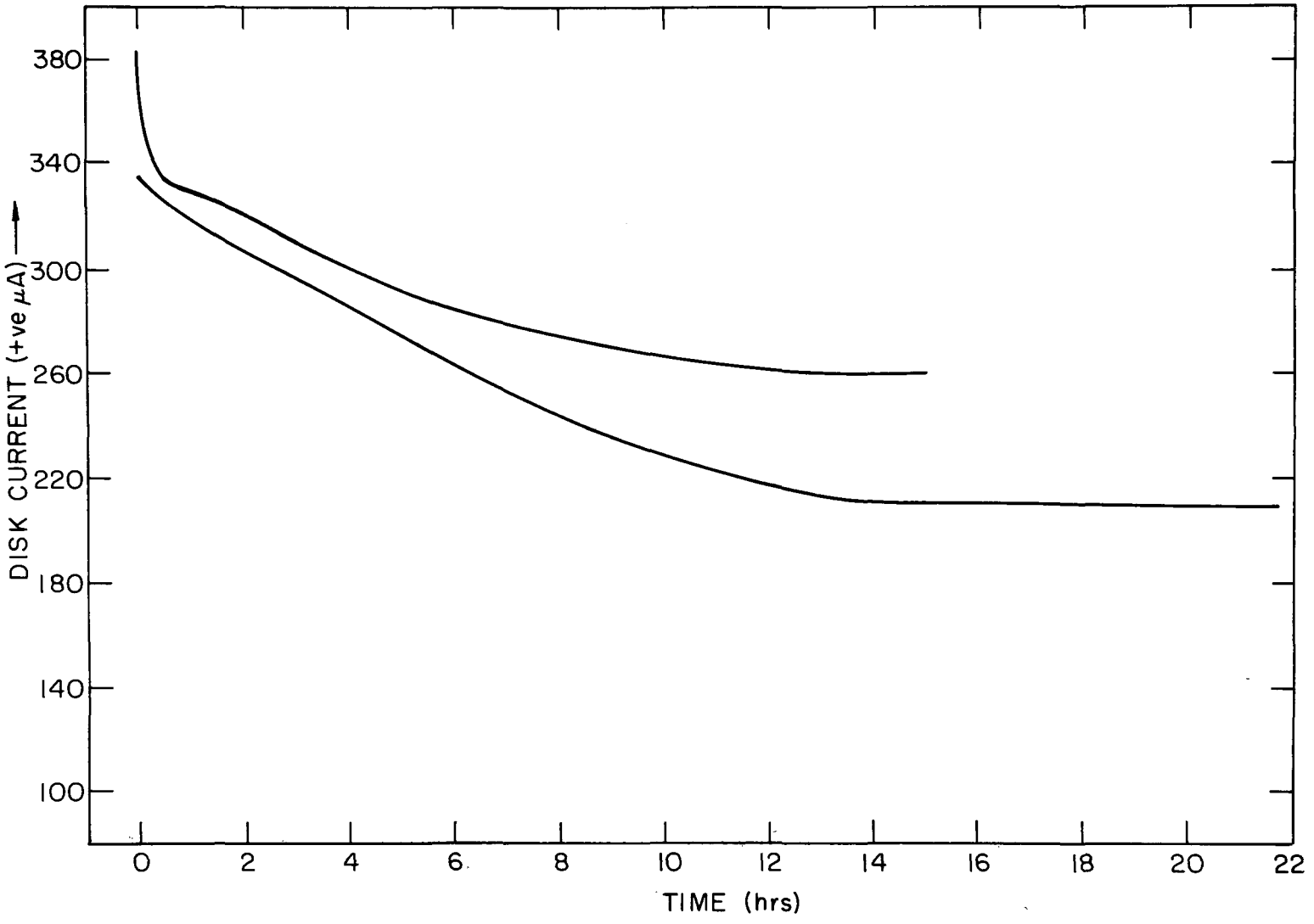

Fig. 18. Current decay during Fe^{2+} oxidation in chemical AMD containing 10^{-2}M Fe^{2+} in 0.02M H_2SO_4 on a vitreous carbon electrode (A, initial decay; B, after cathodic cleaning step)

reaches 55% of its original value after 36 hr in the plateau region. Since the electrode can be cathodically regenerated (-0.90 V), the indications are that either some surface oxide accumulates on the surface and inhibits the oxidation process or that small quantities of impurities (cathodically reducible) in our solutions diffuse to the electrode and have a similar poisoning effect.

Data were then taken for various synthetic AMD waters; current transients were measured in each case with the electrode held at +1.2 V. Fig. 19 shows the transient over a 66-hr period in synthetic AMD of pH 2.72 and containing 1.04×10^{-2}M Fe^{2+} (the calculated oxidation current is 312 μA) and 0.73×10^{-2}M Fe^{3+}. The solution was not centrifuged. The initial current is 320 μA and falls to 24 μA after 66 hr. The decrease after 14 hr was 50.6% and after 66 hr it was 92.5%. So in synthetic AMD the same phenomenon is observed as in chemical AMD but to a much larger extent. Now, is the effect due to soluble species or to the suspended solids?

In a centrifuged solution of synthetic AMD containing 2.16×10^{-2}M Fe^{2+} and 1.89×10^{-2}M Fe^{3+}, the initial current was 616 μA (648 μA calculated) falling 66 μA after 14 hr, i.e., an 89.3% decrease. Thus, the phenomenon still occurs, even in these solutions. Cathodic cleaning at -0.90 V only resulted in an increased current to 380 μA.

Since the solutions prepared above were more concentrated than actual AMD and contained more solids, a centrifuged synthetic AMD solution was diluted with 0.02M H_2SO_4. The resulting solution was 2.29×10^{-3}M in Fe^{2+} and 2×10^{-3}M in Fe^{3+}. The calculated limiting current for Fe^{2+} oxidation in this case is 69.4 μA. The transient current at +1.2 V in this solution fell from 70 μA to 53 μA after 14 hr (a 24.3% decrease) and thence to 22 μA (a 68.6% decrease) after 66 hr. Again the same phenomenon was observed but again to a lesser degree.

In summary, it is evident that on the vitreous carbon electrode employed for these electrochemical investigations, the current for Fe^{2+} oxidation to Fe^{3+} decays with time of immersion of the electrode in both chemical and synthetic AMD, but in the latter solutions the rate of decrease is generally less if the originally prepared solution is centrifuged and/or diluted. Thus, after 14 hr at +0.9 V or +1.2 V in chemical AMD, an $\sim$ 30% fall in current is observed compared to a 50.6% fall in uncentrifuged synthetic AMD and 24% in centrifuged and diluted synthetic AMD. After 66 hr, the equivalent decreases were 45%, 92.5% and 69% in chemical AMD (10^{-2}M Fe^{2+}), uncentrifuged synthetic AMD (1.04×10^{-2} and 0.73×10^{-2}M Fe^{3+}) and centrifuged and diluted synthetic AMD (2.29×10^{-3}M Fe^{2+} and 2×10^{-3}M Fe^{3+}), respectively.

It was also found that an increase in rotation speed of the electrode in chemical AMD causes a sharper drop in current with time. In centrifuged synthetic

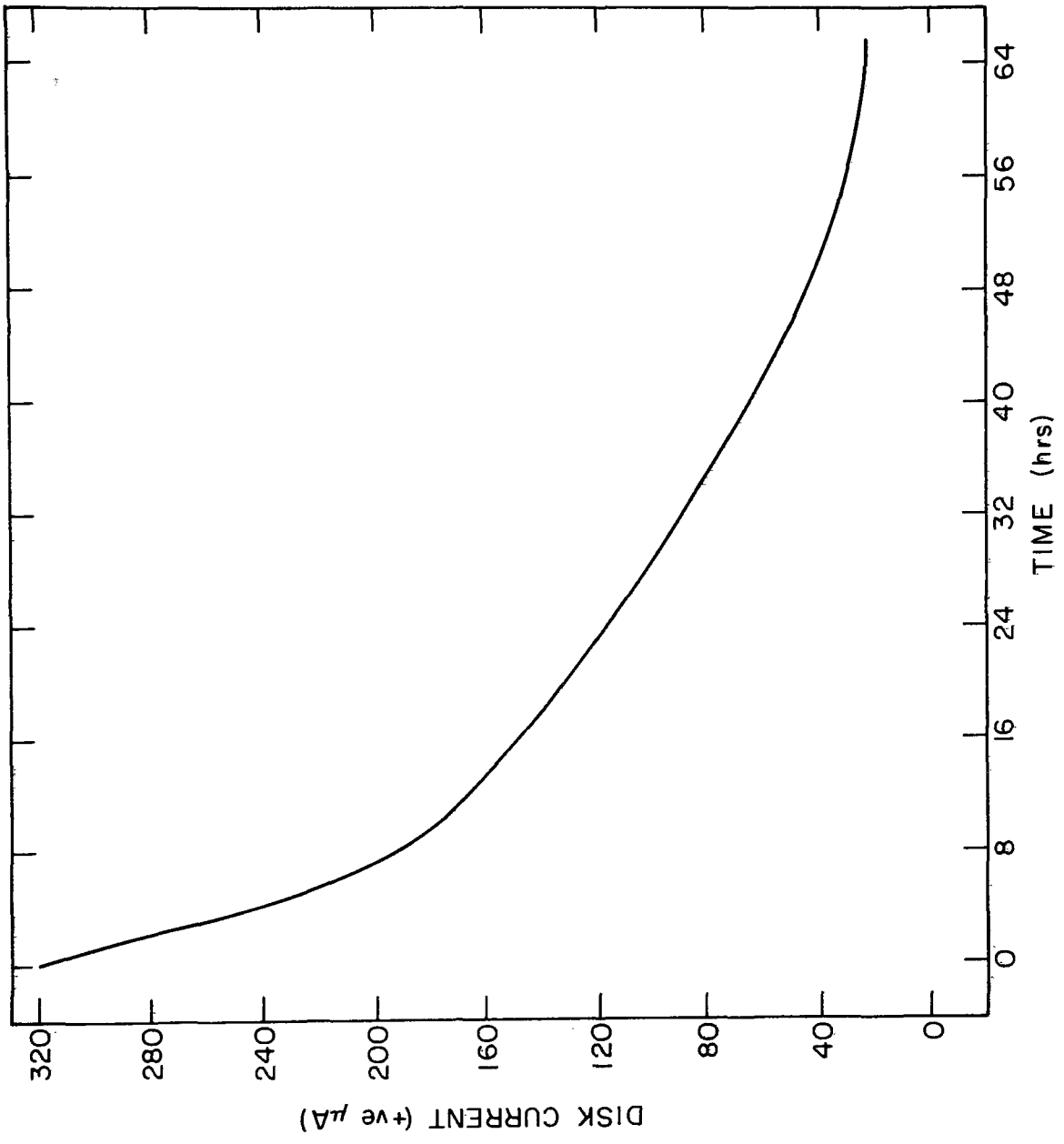

Fig. 19. Current decay during Fe^{2+} oxidation in uncentrifuged synthetic AMD containing 1.04×10^{-2}M Fe^{2+} as well as 0.73×10^{-2}M Fe^{3+} in H_2SO_4 of pH 2.72 on a vitreous carbon electrode held at +1.2 V and 23 rps

AMD containing 1.88×10^{-2}M Fe^{2+} and 1.62×10^{-2}M Fe^{3+}, the rate of fall of current was 1.9 μA/min at a rotation speed of 12.1 rps; at 35.1 rps, the rate of fall was 6 μA/min. This, together with the observations that the electrode can be cathodically cleaned at -0.9 V (the optimum time here appears to be 5 min) suggests that the electrode is being poisoned by a soluble reducible impurity. Formation of some surface oxides may also contribute to the observed decreases. The indications are that the poisons can be removed by cathodic pulsing of the electrode. Application of large (2.0 V) anodic overvoltages certainly does not enhance performance of the electrode.

ANOLYTE SEPARATION

It has been shown that reduction of anodically generated Fe^{3+} back to Fe^{2+} occurs on a 316 stainless steel cathode at < -0.15 V (SCE). This finding has also been confirmed in a laboratory scale reactor. Because of this, a membrane is required to separate anode and cathode; the following properties are necessary:

1. Acid stability
2. Low ohmic resistance
3. Substantial impermeability to dissolved Fe^{3+}
4. Permeable to Fe^{2+}

One candidate material (1-mil thickness) was obtained from RAI Research Corporation (L.I. New York).

Acid Stability: To test for this property, a sample of the membrane was immersed in 0.02M H_2SO_4 and examined at various intervals up to 1 month total immersion. The examination was a simple visual one and in addition a test of mechanical strength was carried out using an Instron Tensile Tester. The latter gives a value of the utlimate tensile strength of materials by destructive testing (i.e., pulling the membrane apart and measuring the load required to do this). A simple visual examination showed no change in the membrane after immersion. An ultimate tensile strength of 3666.7 psi was indicated for the immersed specimen which is to be compared with 3895.2 psi for a sample of the membrane which had not been immersed. It is concluded that the membrane is stable in these acid solutions.

Ohmic Resistance: This property was evaluated with a conductivity bridge (model no. R.C. 16B2, Industrial Instruments, Inc., Cedar Grove, N.J.). A plexiglass conductivity cell was constructed which had provision for insertion of the membrane to divide the cell in two. When positioned, no conducting path between two Pt electrodes was available in the 0.02M H_2SO_4 solutions on either side of the membrane, other than through the membrane.

The resistivity of the 0.02M H_2SO_4 was measured in the absence and in the presence of the membrane. In the former case, a resistivity of 96.2 ohm-cm was indicated and in the latter case the value increased slightly to 106.4 ohm-cm. A previously determined value for the resistivity of 0.02M H_2SO_4 was 104.6 ohm-cm. It is clear then that the membrane has a very low ohmic resistance and thus will not significantly increase iR loss in a practical cell in which it is present.

Impermeability to Dissolved Fe^{3+}: The same conductivity cell was also used for these measurements. The membrane was used to separate solutions of "Fe^{3+}-free" 0.02M H_2SO_4 on the one side and a solution of 4×10^{-2}M Fe^{3+} in 0.02M H_2SO_4 on the opposite side. This setup was left to stand for 11 days and the 0.02M H_2SO_4 initially containing no Fe^{3+} was then tested for Fe^{3+} by titration with $K_2Cr_2O_7$ using diphenylamine sulfonate as indicator. Though the test is sensitive to 5 ppm, no Fe^{3+} species were found. It is concluded that the membrane is impermeable to Fe^{3+}.

Permeability to Fe^{2+}: This property was tested in the same cell. One side of the cell contained 0.02M H_2SO_4 and the other side contained 10^{-2}M Fe^{2+} dissolved in 0.02M H_2SO_4. After 8 days, the 0.02M H_2SO_4, originally containing no Fe^{2+}, was titrated for Fe^{2+} with $K_2Cr_2O_7$, using diphenylamine sulfonate as an indicator. The titration showed that Fe^{2+} had diffused through the membrane to give a concentration of 2×10^{-4}M Fe^{2+}.

To further test the selectivity of the membrane, 0.02M H_2SO_4 was placed on one side of the cell, with a mixture of 5×10^{-2}M Fe^{2+} and 5×10^{-2}M Fe^{3+} in 0.02M H_2SO_4 on the other side. After 11 days, titrations indicated that whereas no Fe^{3+} had diffused through the membrane, the concentration of Fe^{2+} in the H_2SO_4 which had originally been iron free was now 8.2×10^{-4}M Fe^{2+}.

It is apparent then that not only is the membrane impermeable to Fe^{3+}, but it also selectively discriminates between Fe^{3+} and Fe^{2+} species, allowing the latter to diffuse through. A computer analysis had been carried out previously on the distribution of the various soluble iron species present in chemical AMD as a function of pH. This had shown that the dominant ferrous species is Fe^{2+} while, depending on pH, the principle ferric iron species are the $Fe(SO_4)^+$ complex and the bare Fe^{3+}. The amount of ferric iron present as hydroxyl complexes is a pronounced function of pH; a pH change of 2.58 to pH 1.8 lowers the concentration of $Fe_2(OH)_2^{4+}$ (mol % total Fe) from 10.6 to 0.72%. Most likely the membrane distinguishes between the two Fe species on a size basis alone, i.e., the ferric iron is much larger because of its complexation in solution and does not permeate through the membrane.

Performance in Synthetic AMD: The membrane was next tested in synthetic AMD prepared in the laboratory from waste coal (containing 1.15×10^{-2}M Fe^{2+} and 9.65×10^{-3}M Fe^{3+} at pH 2.67). On one side of the cell was placed

fresh 0.02M H_2SO_4 and on the other was placed the above, uncentrifuged, synthetic AMD. At the end of 9 days, the fresh 0.02M H_2SO_4 was tested for iron content. This solution originally containing no Fe^{2+} and no Fe^{3+} was now found to contain 4.25×10^{-4}M Fe^{2+} but still no Fe^{3+}. The results of the experiments in chemical AMD are confirmed. Also, over a 32-day period in the synthetic AMD, no disintegration in mechanical properties of the membrane was found. It is concluded that the membrane is an emminently practical material for use as a separator for anode and cathode in an operational electrochemical AMD unit.

The following is a list of those conclusions, based on the work described in this section of the report, which are relevant to the development of a practical AMD treatment process.

1. The anodic oxidation of Fe^{2+} to Fe^{3+} does take place on a carbon electrode at a mass transport limited rate; the oxidation region is about 0.80 V in extent; the potential plateau for this process is shifted to more positive values by increasing the Fe^{3+} concentration; this shift (< 0.2 V) is not sufficient to cause problems in an operational system.

2. Excessive oxidation (high positive potentials) at the carbon electrode will inhibit somewhat the Fe^{2+} oxidation; this will not cause a problem in a practical reactor, since such high positive potentials will not be reached.

3. Hydrogen evolution occurs on a polished 316 stainless steel cathode (in deaerated 0.01, 0.02M H_2SO_4) at potentials more negative than -0.5 V (SCE); these currents are not diffusion limited but are controlled by a slower electrochemical kinetic step.

4. The cathode in 0.02M H_2SO_4 is passivated by an oxide film at potentials more positive than -0.04 V; this film is removed only at potentials more negative than -0.90 V the normal operating region of the cathode.

5. The diffusion limited back reduction of Fe^{3+} to Fe^{2+} occurs at potentials more negative than -0.15 V.

6. Soluble ferric iron is reduced to the metal on a 316 stainless steel cathode in 0.02M H_2SO_4 at potentials $\leq$ -1.0 V; large currents from H_2 evolution can be supported before iron deposition occurs.

7. A highly selective membrane is available which will prevent the penetration of Fe^{3+} specie while still passing Fe^{2+}; the membrane has acceptable ohmic and structural characteristics.

8. Smooth carbon electrodes show a slow degradation in performance as the result of poisoning by soluble species; the degradation is enhanced in AMD water prepared from waste coal; the degradation has not been detected with porous carbon electrodes.

SECTION 5

ELECTROCHEMICAL REACTOR CONFIGURATION

The economics of any large scale electrolytic process are dependent upon the capital costs of the electrolysis cells. Obviously, for a given set of electrode materials, the smaller the required electrode area, the less expensive will be the system. For the total process being considered here, i.e.,

$$Fe^{2+} + H^{+} + \text{electrical power} \rightarrow Fe^{3+} + 1/2\ H_2$$

the overall area of the electrodes is determined by the rate of diffusion of Fe^{2+} to the anode-electrolyte interface. To a first approximation, this diffusion rate is proportional to the concentration of Fe^{2+} in the bulk electrolyte and to the diffusion coefficient of the hydrated Fe^{2+} ions. The rate is inversly related to the thickness of liquid boundary adjacent to the electrode surface.

The diffusion coefficient is an inherent property of the AMD solution and is not amenable to external control. The concentration of Fe^{2+} is fixed by the specific AMD water being treated and by the desired conversion factor. Thus the only variable available for experimental manipulation is the distance Fe^{2+} must diffuse in order to react on the electrode surface. (In this treatment, mass transport mechanisms such as convection are considered as techniques for reducing the diffusion boundary layer and are essentially specified by the reactor configuration.)

Three reactor configurations (simple parallel electrodes, fluidized bed electrodes, and packed bed electrodes) were evaluated in the context of minimizing this diffusion boundary layer and hence the eventual size of an electrolytic cell. Specifically, the investigation of each configuration involved the reduction of experimentally measured reactor performance to an analytical equation. Then, choosing a "typical" AMD concentration and an acceptable conversion factor, these equations were used to compare the reactor types via a minimum geometric anode area.

EXPERIMENTAL

All the experimental engineering investigations were performed in a small pilot plant constructed entirely of glass and 316 stainless steel. The electrolytic reactor was formed inside a 4 in. glass pipe lined with a 1/2 in. thick graphite anode; a smaller column was available for preliminary studies of fluidization phenomena. The system was designed so that variations in reactor length and electrode geometry could be made without excessive downtime.

At 100 A (the current capability of the power supply) the maximum possible AMD flow (0.02M Fe^{2+}) for 100% conversion is 48.5 gal/hr. A high speed Teflon gear pump, together with a variable bypass stream, provided a smooth, nonpulsating flow from a 200 gal polyethylene tank. Flow through the reactors was controlled and measured by valved rotameters below the columns.

All experiments were performed using a chemical AMD solution containing either 0.01 or 0.02M Fe^{2+} and 0.02M H^{+}. The stock solution was prepared and stored in the 200 gal tank incorporated in the system. The principal system variables were flow rate and current. Iron (total and Fe^{2+}) was determined via standard techniques. A periodic check was made on the stock solution to determine if any Fe^{2+} oxidation (from dissolved air) was occurring spontaneously; no Fe^{3+} was found.

For all runs, the Fe^{2+} conversion was determined after the effluent had reached a constant concentration. Although it was desired to measure the rate of hydrogen production by means of a wet test meter, it was found that the gas production rate (at these low currents) was too far below the range of the instrument to permit reliable readings.

ANNULAR FLOW REACTOR

The basic annular flow reactor contained a 3 in. diameter carbon anode and a 2.875 in. stainless steel cathode. The effective column length was 4 ft (120 cm). The cathode was wrapped with a single layer (0.010 in.) of porous polyethylene felt in order to prevent shorting to the close spaced anode.

Table 1 presents the data obtained for a typical test run. The flow rate was 1.7 gal/hr. The current was varied stepwise and the indicated final Fe^{2+} concentration was measured. Cell voltages are not presented since they

represent mostly iR losses in the current leads and are thus specific to this single experimental setup.

Table 1. Conversion Data for a Flow of 1.7 Gal/Hr

Current, Amperes	Final Fe^{2+} Concentrations, M	Conversion, %	Current Efficiency, %
0.5	0.0174	12.5	100
0.75	0.0162	19	100
1.00	0.0153	24	93
2.00	0.0136	31	60
3.00	0.0130	35	49

The increased ferrous oxidation at the higher currents (1 ampere and above) results from the oxidation of Fe^{2+} by oxygen evolved at the carbon anode. Note that, although higher Fe^{2+} conversions are now possible, the process is relatively inefficient.

These data were then compared to the results predicted by applying a suitable mass transfer equation to the experimental reactor configuration. A correspondence in results would establish the validity of the mass transfer equation as used for the system under study. The general equation[9] for the diffusion limited current in annular flow (for a one-electron process) is:

$$i_{lim} = 0.85\, F D_i C_\infty \left[\frac{\langle V \rangle \phi}{(1 - k)\, r\, D_i X} \right]^{1/3} \qquad (11)$$

where

F = 96,500 A-sec/equivalent

D_i = diffusion coefficient of species i

C_∞ = local bulk concentration

$\langle V \rangle$ = flow velocity

r = radius of the outer tube

X = distance from the leading edge

k = radius of innerelectrode/radius of tube

The diffusion coefficients used were 5×10^{-6} mol/cm^2-sec for Fe^{2+} and 2×10^{-6} mol/cm^2-sec for Fe^{3+}. It was shown in the rotating disk experiments (Section 4) that these coefficients reasonably well described the diffusion of Fe^{2+} and Fe^{3+}, in 0.02M H_2SO_4.

The quantity of ϕ is a tabulated geometric parameter, which describes the effect of different annular configurations on the limiting current. As can be seen, the limiting current is directly proportional to the bulk concentration and inversely proportional to the cube root of the distance from the upstream edge of the annulus.

For the type of annular flow being considered, the limiting current is essentially infinite at the upstream edge of the anode where a fresh solution is brought in contact with the electrode. The limiting current drops as the hydrodynamic boundary layer increases in thickness and as the bulk concentration begins to fall. In the lower part of the column, the growth of the boundary layer limits the maximum current. In the upper portion, the boundary layer reaches a relatively steady thickness and the change in the bulk concentration controls the limiting current.

For a given annulus geometry and flow rate, the above equation can be solved using an incrementally determined bulk concentration. The bulk concentration is computed by a simple mass balance and the value used to compute the new limiting current. The entire concentration profile for a column of arbitrary length can be rapidly calculated using a computer.

The computer program (written in DCAL) shown in Table 2 was used to provide analytical confirmation of the experimental data obtained from the pilot plant.

The program first requires the major input variables (step 1.2): the flow rate in gal/hr (FLOW), the radius of the anode (ROUT). After computing the flow area and velocity, the program requests the value of the geometric parameter ϕ (PHI) in step 2.2. In step 2.45, the initial concentration of Fe^{2+} (ICONC) is converted into a charge per unit volume basis. The initial limiting current is calculated in step 3.1 according to Eq. (10)described above. Step 3.15 takes into account the existence of the ferric to ferrous back reduction which, as shown, occurs at the cathode. Step 3.2 computes the quantity of charge passed in the first centimeter of column height using the previously calculated limiting current. Steps 3.4 and 3.5 compute a new concentration to be used in the next iteration. The calculations continue until the concentration profile for the entire column is developed (steps 2.6 and 3.6). The computed concentration profile for a flow rate of 1.7 gal/hr is shown in Table 3 below.

Table 2. Computer Program for Evaluation of Annular Flow Data Obtained with Pilot Plant

```
1.1 FLOW=0, RIN=0, ROUT=0, PHI=0
1.2 DEMAND FLOW, RIN, ROUT
1.25 AREA=PI*((ROUT^2)-(RIN^2))
1.3 VELOC= (FLOW*.163)/AREA
1.4 KAP=RIN/ROUT
1.5 DO PART 2
2.1 TYPE KAP, AREA
2.2 DEMAND PHI
2.3 TCHARGE=0, I3LIM=0, ITLIM=0, PCHARGE=0, NCHARGE=0, I2LIM=0
2.4 DEMAND DIST,CONC, ICON
2.45 ICHARGE= ICONC*96500000*6.45*AREA
2.5 TYPE "CONCENTRATION PROFILE AT   GALLONS/HOUR
            HEIGHT(CM)    CONCENTRATION(M)    CURRENT(MA/CM)"
2.6 DO PART 3 FOR DIST =DIST BY 1 TO 120
3.1 I2LIM=((24.1*CONC*PHI*(DIST^(-.333)))*((VELOC/((1-KAP)*ROUT*
      2.54))^.333))
3.15 I3LIM=((13.1*(ICONC-CONC)*PHI*(DIST^(-.333)))*((VELOC/((1-
KAP)*RIN*2.54))^.333))
3.16 ITLIM=ITLIM+I2LIM
3.2 PCHARGE= 5080*PI*ROUT*(I2LIM-I3LIM)*(VELOC^-1.0)
3.3 TCHARGE=TCHARGE+PCHARGE
3.4 NCHARGE=ICHARGE-TCHARGE
3.5 CONC=(ICON*NCHARGE)/ICHARGE
3.6 TYPE IN FORM 1: DIST, 1000*CONC, 1000*I2LIM, IF FP DIST/10=0
3.7 TYPE IN FORM 2: ITLIM/120*2871 IF FP DIST/120=0

FORM 1:
                %%%          %.%%%%                  %.%%
FORM 2:
    REQUIRED CURRENT= %%.%% AMPERES
```

Table 3. Concentration Profile at 1.7 Gal/Hr

Distance, cm	Concentration, M
10	0.0192
20	0.0188
30	0.0184
40	0.0181
50	0.0178
60	0.0175
70	0.0172
80	0.0170
90	0.0168
100	0.0166
110	0.0164
120	0.0162

The predicted final concentration of 0.0162M agrees with the maximum observed conversion at 100% current efficiency. Further confirmation of the applicability of the analytic equations used was obtained by extending the data to include a wide range of flow rates. These results are shown in Table 4. Here again, the agreement between the experimental and analytical values is excellent.

Table 4. Final Fe^{2+} Concentrations as a Function of Flow Rate

	Fe^{2+} Concentration, M		
		Predicted	
Flow, gal/hr	Observed	No Back Reduction	Back Reduction
5	0.0184	0.018	0.018
2.5	0.0173	0.0168	0.0170
1.7	0.016	0.0160	0.0162
1.0	0.016	0.015	0.0154
0.5	0.0132	0.012	0.013
0.26	0.010	0.0092	0.0096
0.0	0.007	0.00	0.0071

The effect of the competing back reaction (the reduction of Fe^{3+} on the cathode) is apparent. The predicted maximum conversions indicate that this back reduction of Fe^{3+} does not become of major significance until the total conversion reaches 50%. Since conversions in excess of 90% are desired, it is apparent that a means of suppressing the competing back reduction is required. As is shown in Table 5, where the computer predicted concentration profiles for a flow of 0.1 gal/hr are compared, conversions of 75% or more can be obtained in relatively short reactors operated at low flow rates once the ferric to ferrous back reduction is suppressed.

Consideration of several alternative approaches to eliminate this reactor inefficiency led to an evaluation of ion selective membrane materials. A polyolefin based material produced by RAI Industries was found to fulfill the basic requirements of stability in dilute sulfuric acid solutions, low ohmic resistance (i.e., permeability to solvated protons and anions), reasonably low cost, and a low permeability for hydrated ferric ions.

Table 5. Concentration Profiles for a Flow of 0.1 Gal/Hr

Distance, cm	No Back Reduction Concentration, M	Back Reduction Concentration, M
10	0.0154	0.0157
20	0.0130	0.0137
30	0.0113	0.0124
40	0.0099	0.0114
50	0.0088	0.0107
60	0.0079	0.0102
70	0.0072	0.0097
80	0.0065	0.0093
90	0.0059	0.0090
100	0.0054	0.0088
110	0.0050	0.0086
120	0.0045	0.0084

FLUIDIZED BEDS

In a fluidized bed, the continuous agitation of glass beads suspended in the interelectrode space by the AMD flow reduces the thickness of the diffusion boundary layer (δ) and thus increases the limiting current density. A further advantage of a fluidized system lies in the elimination of the hydrodynamic boundary layer which is present in a simple flow system.

The experimental configuration was similar to that described above. The carbon anode was 2 ft long and had an internal diameter of 3 in. The stainless steel cathodes were 0.84 and 1.90 in. in diameter. Since wall effects on fluidization velocity are not important, these variations in annular size permit the fluidization of a wider range of bead sizes than could be possible if the reactor geometry were fixed. All experiments shown were performed with commercial grade glass beads, (Cataphote Corp.). The particle size given thus represents an average value.

Note that the bead size and the liquid velocity cannot be independently varied, since each size bead requires a specific liquid velocity for fluidization. The fluid velocity at 65% bed voidage ranges from 0.05 cm/sec for 35 μ beads to 2 cm/sec for 375 μ beads. A graph of fluid velocity (at a measured 65% bed voidage) versus particle diameter is shown in Fig. 20; the observed velocity varies as the average particle size to the 1.54 power. These results are in excellent agreement with the data of Saxon[12] which indicate that a value of 1.59 should apply at constant bed voidage.

Table 6 presents the experimental data for the treatment of chemical AMD (1000 mg/ℓ Fe^{2+}, 2000 mg/ℓ H^{+}). The actual current passed through the reactor was consistent with the theoretical current calculated on the basis of the observed ferrous to ferric conversion. For each experimental point, the reactor was operated at constant current until the effluent Fe^{2+} concentration reached a steady value.

The quantity of glass beads in the bed was adjusted so that at the required bed height (2 ft) bed voidage would be 65%. This value has been shown to result in optimum mass transfer rates.[13] Note that in the case of the larger (and hence more mobile) beads, conversions are now approximately a factor of 20 times greater than a simple annular reactor of equal anode area.

Table 6. Fluidized Bed Data

Flow Rate, gal/hr	Bead Size, μ	Current, amps	Final Fe^{2+} Concentration, M	Conversion, %
34.3	375	9	0.017*	12
20	200	5	0.0176†	12
1.2	35	1	0.0112†	44

*(initial 0.0193).
†(initial 0.02).

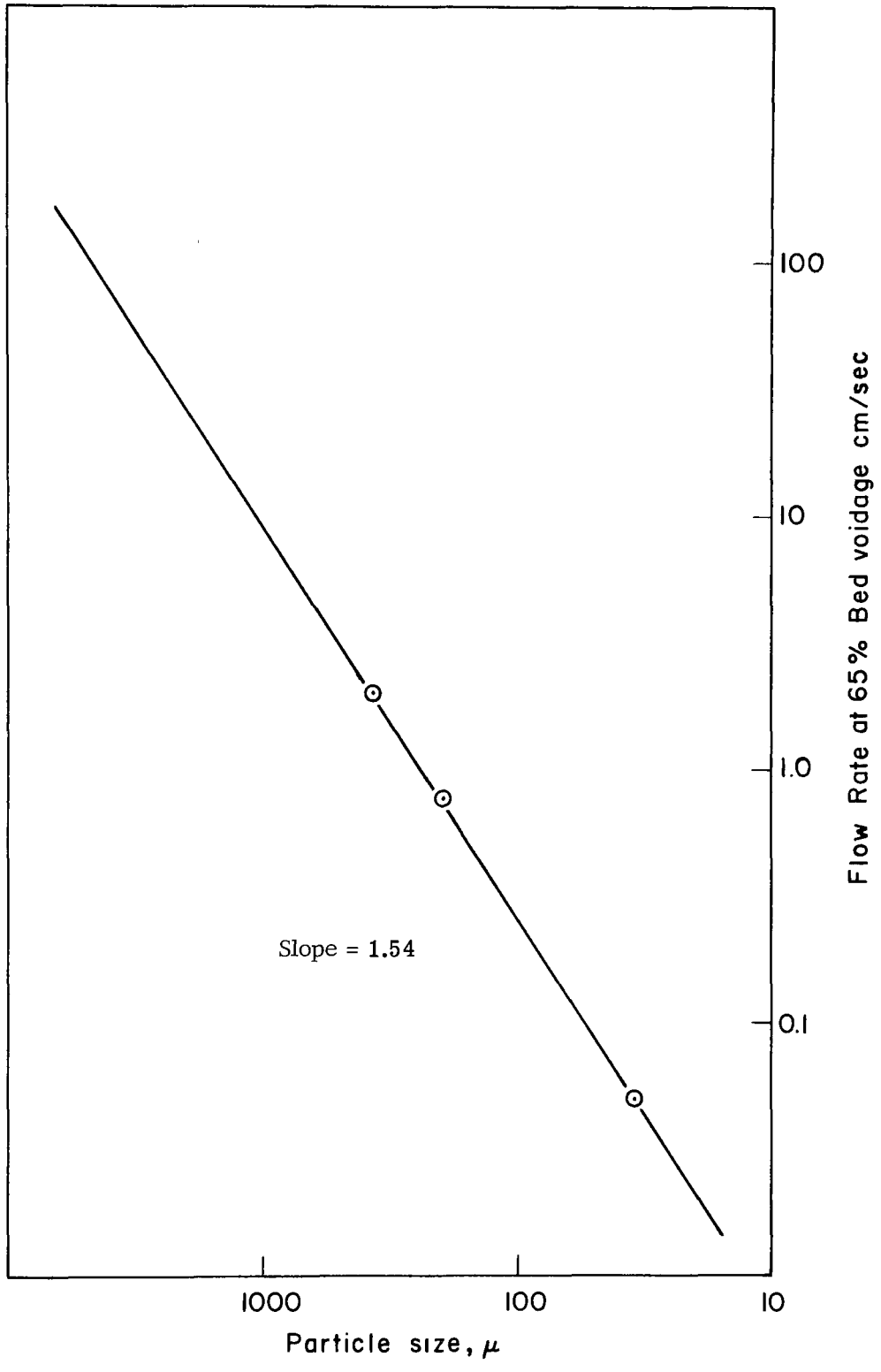

Fig. 20. Plot of fluid velocity versus particle diameter at 65% bed voidage

Since in these experiments no membrane was used around the cathode, the back reduction of ferric ion must be considered in evaluating the effectiveness of the apparatus.

In these experiments, conversions approaching the desired 95-99% were not obtained. According to the subsequent analysis, this was primarily because the reactor length was too short for the flow rates being employed. It was shown subsequently that in the case of the 35 μ beads, a column 320 cm long would have been needed to produce a Fe^{2+} conversion above 95%. The alternative of using bead sizes below 35 μ was not feasible due to entrainment of the very fine particles.

ANALYSIS

Mass transfer correlations for liquid fluidized beds are not available. We have therefore used the following theoretical model of the configuration to assist in analysis of the experimental data. In a fluidized bed, the local limiting current density is presumed to be proportional to the local concentration of the reacting specie. In other words, although the height of the bed affects the overall conversion, the local current density is not a function of position. It is, therefore, possible to represent the local limiting current by an equation of the form:

$$\text{ILIM} = \text{FKON} \cdot \text{CONC} \tag{12}$$

where:

ILIM = the local limiting current (amps/cm^2)

FKON = a proportionality factor which is constant for a given reactor geometry, a bead size and flow rate

CONC = the local concentration (mol/ℓ)

This equation should be compared to Eq. (13) below, which expresses the limiting current in stagnant solutions Eq. (5).

$$\text{ILIM} = \frac{n F D}{\delta} \text{CONC} \tag{13}$$

where:

n = number of electrons transferred

F = 96,500 AMP-SEC/equivalent

D = diffusion coefficient

δ = boundary layer thickness (cm)

CONC = concentration (mol/cm^3).

Note that if a value for the coefficient of performance (FKON) is known, a value for the equivalent boundary layer thickness in the fluidized system can be computed as shown below.

$$\delta = \frac{n\ F\ D}{1000 \cdot FKON} \tag{14}$$

For the reaction $Fe^{2+} \rightarrow Fe^{3+} + e^-$, Eq. (13) reduces to:

$$\delta = \frac{0.5 \times 10^{-3}}{FKON} \tag{15}$$

Using the experimental data shown above, values for the constant FKON were calculated via an iterative computer program (Table 7) developed specifically for this purpose. Since for each point the flow rate and the final and initial Fe^{2+} concentration are known, the unique value of FKON which satisfies these boundary conditions can be established. In addition, the reverse procedure, i.e., predicting concentration profiles for other size reactors, can also be readily accomplished.

FKON is first given an initial value which is used to perform an incremental material balance along the length of the column. Successive estimates of FKON are made until the predicted value of the final ferrous concentration coincides with the experimental value. The program is written in DCAL. In Part 1, the cathode size, the anode diameter, the average particle diameter, the flow rate, and the bed voidage are requested. The flow area and the fluid velocity are then computed. Part 2 requires the reactor length and the initial and final ferrous concentrations. Step 2.45 converts the initial ferrous concentration into the quantity of charge present in the first centimeter of the column. Part 3 performs successive material balances up the column. The local current density is calculated in step 3.1 which also corrects for the back reduction of Fe^{3+}. In Part 4, the computed value for the final ferrous concentration is compared with the experimental data. Part 5 computes the particle Reynold's number after the proper value of FKON has been determined. The values so obtained are shown in Table 8.

Table 7. Computer Program for Evaluation of Fluidized Bed Data

```
1.2 DEMAND RIN, ROUT, DPART, FLOW, BVOID
1.25 FAREA=(PI*((ROUT^2)-(RIN^2)))*BVOID
1.3 VELOC=((FLOW*.163)/FAREA)
1.4 DO PART 2
2.1 TYPE IN FORM 1: FAREA, VELOC
2.3 TCHARGE=0, PCHARGE=0, NCHARGE=0, ILIM=0
2.4 DEMAND LENGTH, ICONC, FCONC
2.45 ICHARGE=ICONC*96500*FAREA*6.45
2.5 TYPE IN FORM 2: FLOW
2.6 FKON=.02
2.7 DO PART 3
3.01 DIST =1, TCHARGE=0
3.02 CONC=ICONC
3.1 ILIM=(FKON*CONC)-(FKON*CONC*(1/2.5)*((ICONC-CONC)/CONC)*RIN/ROUT)
3.2 PCHARGE=5080*PI*ROUT*ILIM*(VELOC^-1)
3.3 TCHARGE=TCHARGE+PCHARGE
3.4 NCHARGE=ICHARGE-TCHARGE
3.5 CONC=(ICONC*NCHARGE)/ICHARGE
3.51 DIST =DIST+1
3.52 TO PART 4 IF DIST=LENGHT+1
3.53 TO 3.1
4.1 FKON=FKON+.005 IF CONC>FCONC
4.101 TO 5.001 IF CONC<FCONC
4.2 TO 3.01
5.001 NRE=0
5.01 NRE=((VELOC/30.5)*(3.3E-6*DPART*62.4))/.6E-3
5.1 TYPE IN FORM 3: FKO, NRE
5.2 DONE

FORM 1:

      FLOW AREA              .  ZZZ.Z SQUARE INCHES
      FLOW VELOCITY           ZZ.ZZ CM/SEC
FORM 2:

*     FLOW RATE          ZZZ.Z  GAL/HOUR
FORM 3:

    FACTOR     ZZZ.ZZZ          REYNOLDS NUMBER      ZZ.ZZ
```

Table 8. Fluidized Bed Calculations

Flow, gal/hr	Bead Size, μ	FKON	Particle Reynolds Numbers, $VD_p \rho/\mu$
34.3	375	0.315	8.58
1.2	35	0.0055	0.02
20	200	0.20	1.70

Fig. 21 shows the relationship between the calculated values for the performance coefficient (FKON) and the experimentally determined particle Reynolds number as shown on the graph. The data are well correlated by Eq. (16).

$$FKON = 0.17\, N_{RE}^{0.28} \qquad (16)$$

The upper limits of the above equation are not clear, since the flow rates obtainable in the apparatus were not sufficient to fluidize larger beads. However, based on other work concerning heat transfer in fluidized beds, such a simple relationship is unlikely to hold above a Reynolds number of 100.

The values for the equivalent boundary layer thickness are seen to be less than 0.001 cm at the higher Reynolds numbers. Since a value of 0.05 cm is representative of stagnant systems,[5] the abrasive effect of the glass beads is clearly evident from both an experimental and theoretical standpoint.

PACKED BED REACTOR

In this configuration, the entire anode space was filled with porous, conductive particles in direct contact with the electrode wall (the "feeder" electrode). The intent was to extend the electroactive surface into the bulk of solution thus minimizing the average diffusion required by the ferrous iron. The exact distance over which the electrode potential was effective remained to be determined. It is to be expected, a priori, that the total exposed electroactive surface would be greater than in either of the previous configurations considered.

The anode bed was formed from 4 × 10 mesh carbon granules within a 3 in. diameter carbon cylinder. Bed heights of 1 ft and 2.5 ft were used. The stainless steel cathodes (perforated in order to allow the generated hydrogen

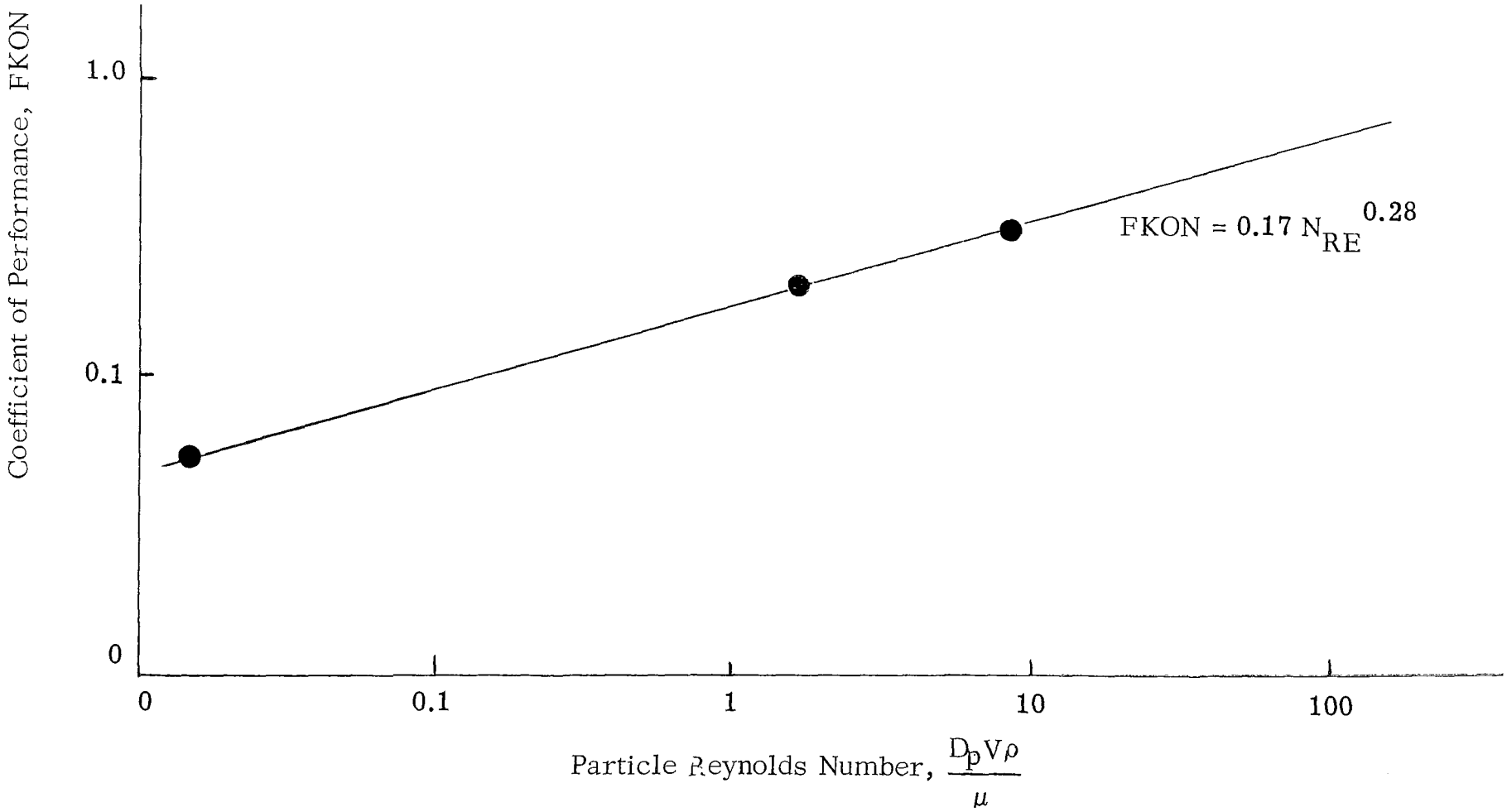

Fig. 21. Correlation of the coefficient of performance with μ the particle Reynolds number

bubbles to leave the reactor without obstructing electrode area) were centrally located along the length of the carbon bed. Cathode diameters of 0.83 and 1.90 in. were used in order to investigate the effect of bed width. For the data shown, the cathodes were wrapped in a single layer of a ferric impermeable membrane.

For each experimental point, the column was operated at constant flow rate and current until a steady effluent concentration was obtained. The Fe^{2+} stock solution (0.01M Fe^{2+}, 0.02M H_2SO_4) was stored in a 200 gal polyethylene tank. The time for each point varied from 5 hr at 1 gal/hr to less than 30 min at 20 gal/hr. Iron concentrations were determined via standard titration techniques.

RESULTS

Figs. 22, 23, and 24 illustrate the basic operating data obtained on packed bed reactors. The results are plotted in terms of the observed ferrous to ferric conversions versus the applied current (expressed as a percentage of the theoretical current required for complete conversion). Data are given for flow rates of 1, 2, 5, 10, 15, and 20 gal/hr. The data in Fig. 22 were obtained at a bed length of 1 ft and a bed width of 1.58 in. Fig. 23 represents runs carried out at the same electrode spacing but with a bed length of 2.5 ft. The effect of changes in bed width from 1.58 in. to 0.55 in. is shown in Fig. 24 for a bed length of 1 ft.

Below a critical mass transfer limitation for each flow rate, the steady state concentrations fall on the 100% efficiency line. When this point is exceeded, most of the excess applied current is consumed in the anodic generation of oxygen. Some of this oxygen produced will oxidize additional Fe^{2+}, but this process is relatively inefficient as can be deduced from the low slope of the operating lines deviating from the 100% efficiency area.

Table 9 compares the mass transfer limitations observed with the 1.08 in. and 0.55 in. bed width. These data were obtained from Figs. 22 and 24.

Table 9. Effect on Column Performance of Changes in Bed Width

Flow Rate, gal/hr	Observed Conversion, %	
	0.55 in. width	1.08 in. width
2	50	47
5	28	27
10	22	20
15	20	-
20	18	-

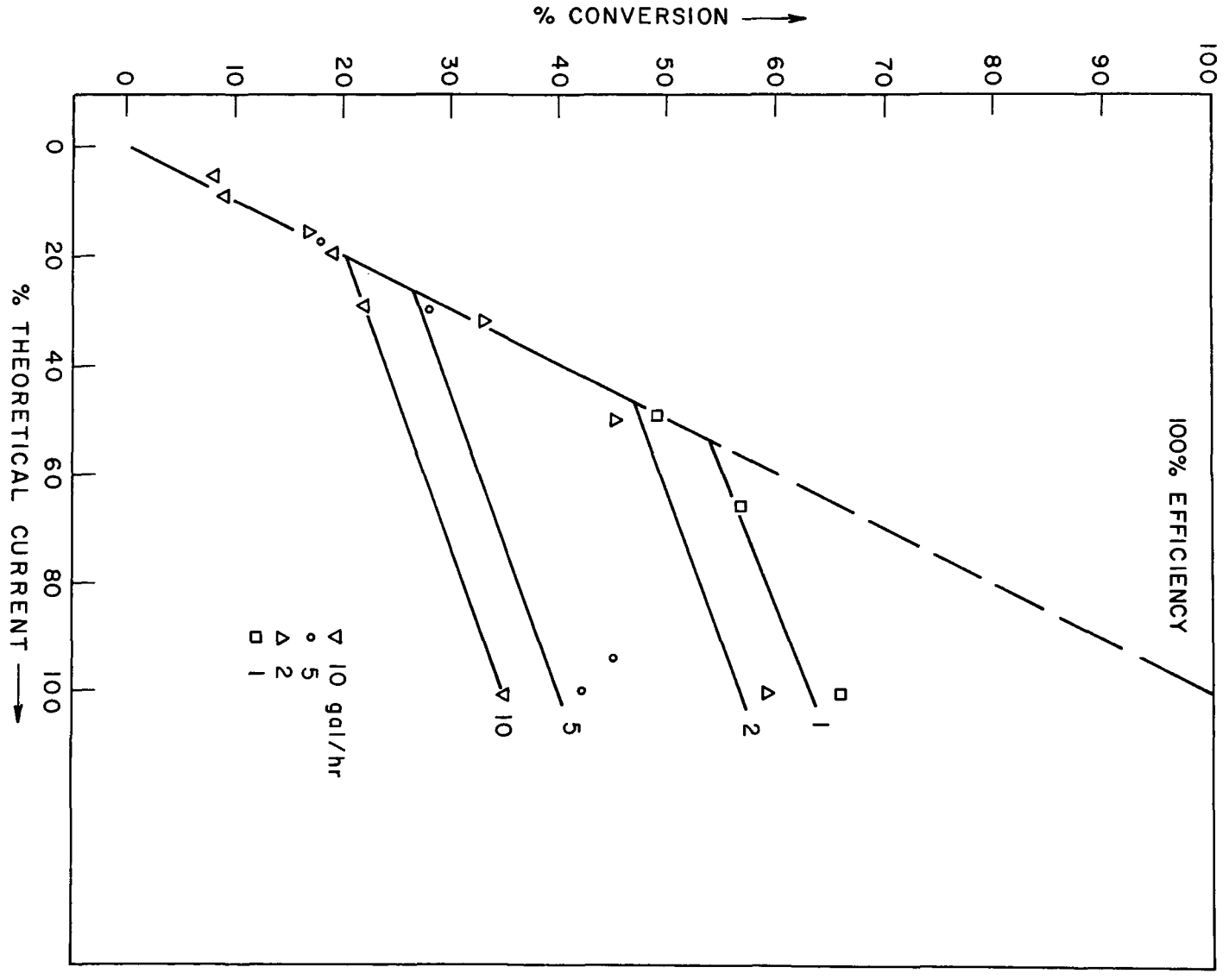

Fig. 22. Packed bed data for a bed width of 1.58 in. and a bed length of 1 ft

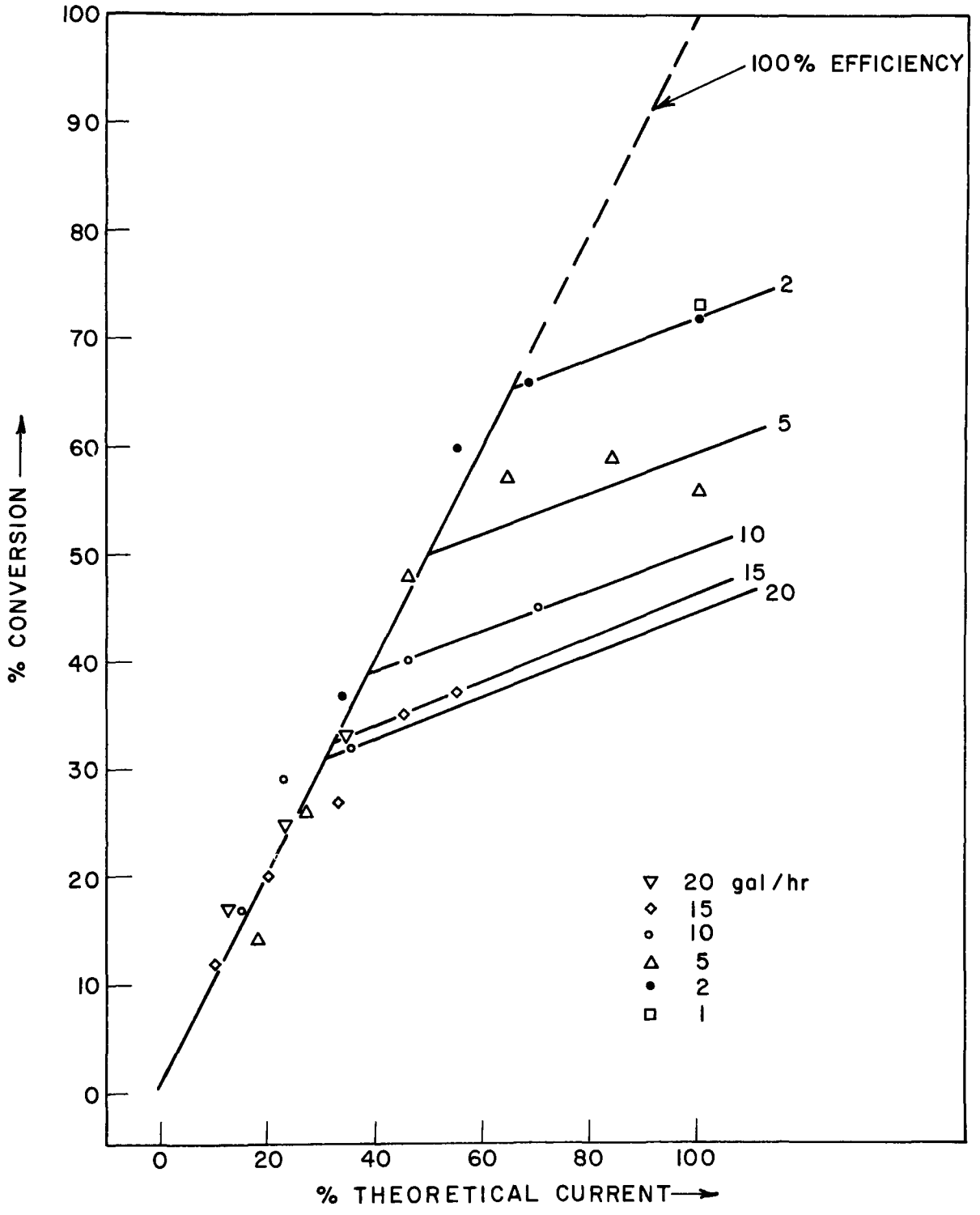

Fig. 23. Packed bed data for a bed width of 1.58 in. and a bed length of 2.5 ft

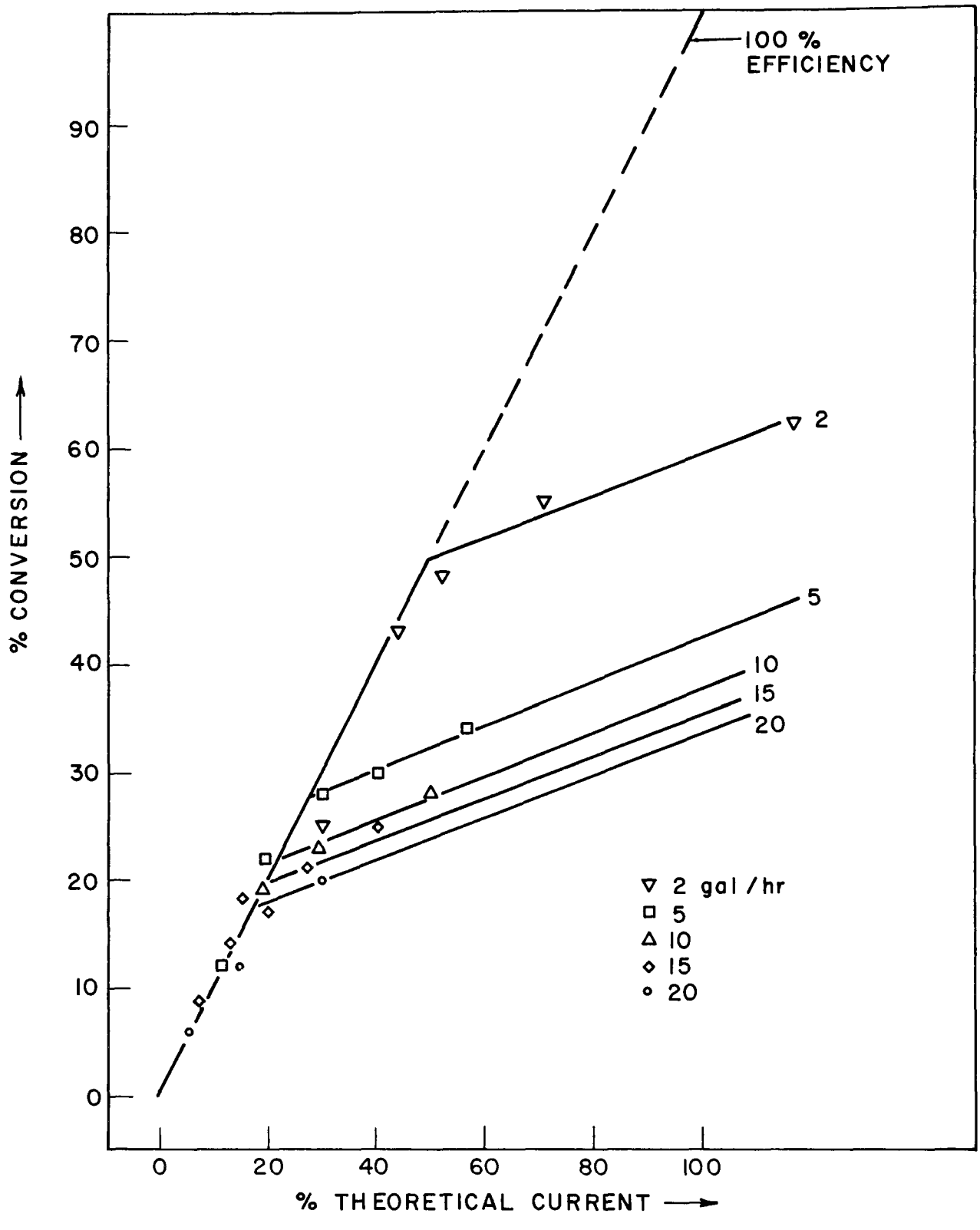

Fig. 24. Packed bed data for a bed width of 0.55 in. and a bed length of 1 ft

Since slightly higher conversions are exhibited by the bed which contains less carbon, it must be presumed that much of the carbon contained in the wider bed is electrochemically inactive. The width of this active carbon zone determines the maximum electrode separation and hence the total area of the stainless steel required in the final reactor.

At a given AMD flow rate, the actual velocity in the bed containing less carbon is higher because of the reduced flow area. Therefore the higher conversions shown in Table 9 are to be expected as a result of increased local turbulence in the fluid surrounding each carbon particle. The next size parameter is bed length.

Table 10 compares the data obtained from the 1 ft (Fig. 22), and 2.5 ft (Fig. 23) columns. The data represent the maximum conversion obtained at 100% current efficiency, i.e., the mass transport limitation of the columns at each flow rate.

Table 10. Effect of Bed Length on Column Performance

Flow Rate, gal/hr	Observed Conversions, %		
	1 ft bed	2.5 ft bed	Exponent
2	47	66	2
5	27	50	2.5
10	20	39	2.5
15	—	33	—
20	—	31	—

If, as expected, the diffusion limiting current for ferrous oxidation is proportional to the ferrous concentration, the effect of bed length on the overall conversion should be given simply by:

$$(1-c)^{\ell} = F \qquad (17)$$

where

c = conversion in a column of unit length

ℓ = number of unit lengths in the column

F = final conversion observed

Computed values, (obtained by plotting the observed conversions versus bed length on log-log coordinates) for the exponent ℓ were given in Table 10.

Since the values determined experimentally are close to 2.5 (the ratio of the column lengths) Eq. (17) should be applicable in predicting the performance of columns of arbitrary length.

Fig. 25 presents the mass transport limited current plotted against flow rate for the region where the overall conversion was relatively constant. These data were obtained from Tables 9 and 10. For liquid flow through packed beds, standard correlations [19] predict a slope of 0.69. The experimental data obtained indicate a value of 0.67. The excellent agreement obtained allows justifiable scaleup to beds operating at higher superficial velocities.

COMPARISON OF REACTOR TYPES

A summary of the pilot-plant data for each of the three reactor configurations considered is shown in Table 11. All the reactors had the same basic inside diameter of 3 in. Since the data points chosen are at currents where significant conversion via oxygen production was not occurring, the currents passed represent the absolute amount of Fe^{2+} that was removed.

It is difficult to compare the three systems directly from these data since the concentrations, flow rates, and reactor sizes are different. However, it is evident that the simple flowthrough reactor cannot compare with the other configurations. In comparing the fluidized bed with the packed bed, it must be noted that the fluidized bed current includes a factor of 2 for the increased Fe^{2+} concentration, a factor of 1.5 ($3.4^{0.4}$) for the increased flow rate, as well as factor of 2 for the reactor length.

A more effective comparison of the three systems can be given in terms of the anode electrode area needed to handle a practical fluid flow. For this purpose, treatment to 95% conversion of the following AMD water was considered: 1000 mg/ℓ of ferrous iron, 0.01M H_2SO_4 at 6,000 gal/hr. The electrode area was computed from the experimentally based extrapolation equations derived above. These comparison data are given in Table 12.

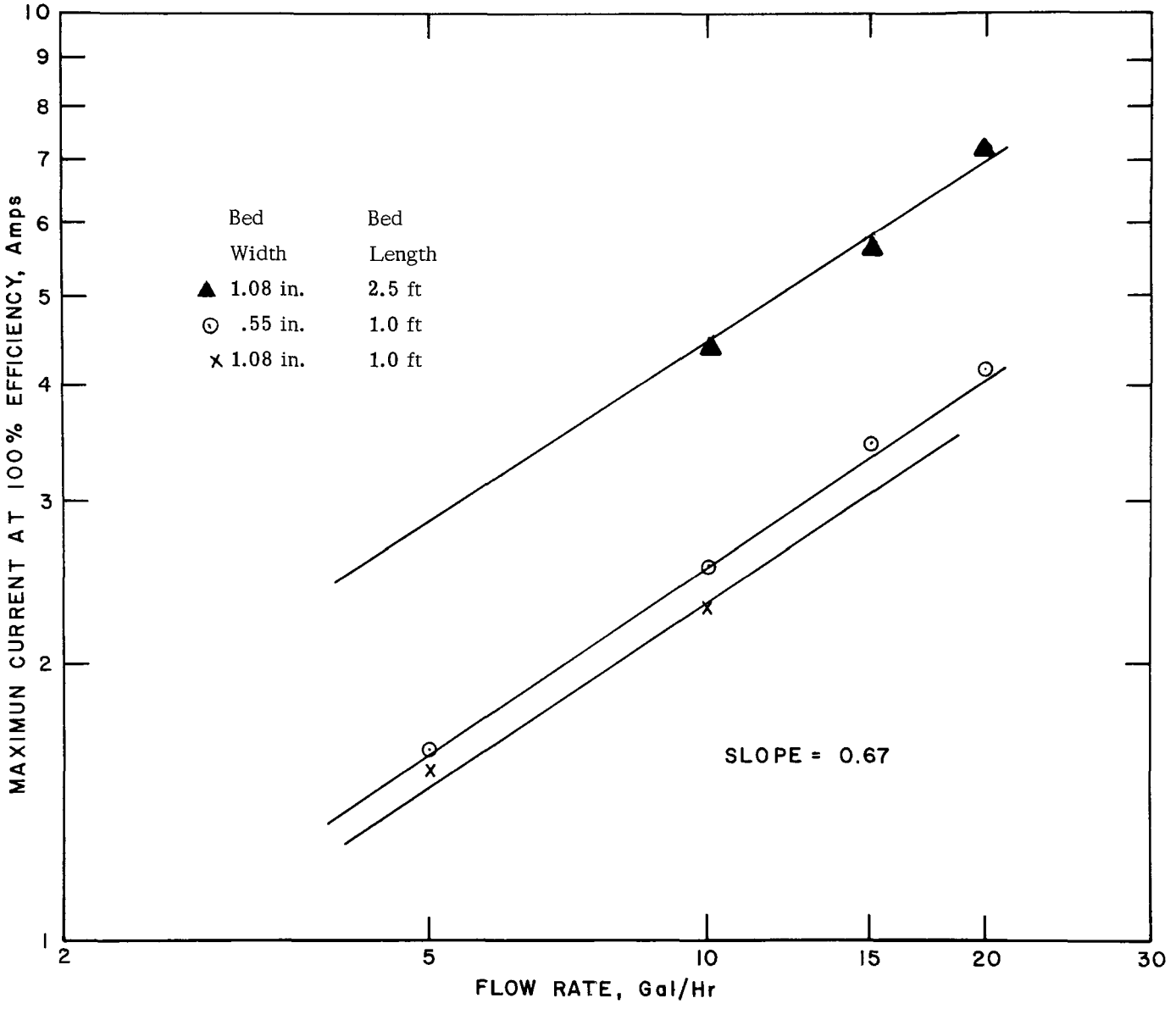

Fig. 25. Settling times of AMD sludges

Table 11. Comparison of Reactor Configurations

Reactor Type	Initial Fe^{2+} Concentration, M	Flow Rate, gal/hr	Conversion, %	Reactor Length, ft	Current Passed, amps
Flowthrough	0.02	5	8	4	1
Fluidized bed	0.02	34	12	2	9
Packed bed	0.01	10	20	1	2

Table 12. Comparison of Electrode Systems Via Anode Size

System	Area, sq ft
Parallel plate	50×10^3
Fluidized bed	6.2×10^3
	$3.25 \times 10^{3*}$
Packed bed	$1.74 \times 10^{3\dagger}$

*Based on value for FKON corresponding to fluidizing 1 mm beds

†Area of stainless steel cathode.

A few more details regarding Table 12 are desirable. The value for the parallel plate system is based on a minimum partial electrode spacing of 0.005 in. since the closer the electrodes, the more efficient the reactor. It is assumed that a ferric iron impermeable membrane can be used; it is also assumed that there will be no problem in feeding solution into the electrolyte gap. Any departure from these assumptions will increase the size of the reactor.

The value of 3.25×10^3 sq ft for the fluidized bed is based on being able to fluidize 1 mm glass beads. The bead size is felt to be the upper practical limit. At 65% bed voidage, the Reynolds number is 100 and the coefficient of performance is 0.6.

The design point for the packed bed reactor was the observed conversion of 17.5% at 20 gal/hr. The electrode area figure in Table 12 is for a reactor consisting of two series connected vertical tanks, each 8 ft high by 3 ft. Each tank is partitioned into 35 flow channels, 1 in. wide and treating 170 gal/hr of AMD.

Clearly then, of the three systems, the packed bed reactor requires the smallest amount of electrode area and should therefore be the least expressive. It is the economics of this system which will be discussed in the following section.

SECTION 6

PLANT DESIGN AND ECONOMICS

The technical basis of the process has been presented in previous sections of this report. Sufficient data have been acquired to justify a first order evaluation of system economics. This is presented below.

Two key items are treated: (1) the cost and configuration of the electrochemical reactor, and (2) the basis for the limestone treatment credits. Finally the economic picture for the entire process is presented.

ELECTROCHEMICAL REACTOR

As the base level design of the packed bed reactor, treatment of 6000 gal/hr of AMD containing 500 mg/ℓ Fe^{2+} is considered. The ferrous concentration was to be reduced to 5% of its original value. The design was based on the pilot-plant data given in Tables 9 and 10. At a flow rate of 20 gal/hr (a superficial velocity of 4.7 gal/hr-in^2), a conversion of 17.5% was observed in a 1 ft column. Possible performance improvements to be derived from operation at higher flow rates were not considered. From Eq. (17), a total column length of 16 ft will be required to accomplish a 95% conversion at this flow velocity. The reactor would be constructed in two series connected vertical tanks, each 8 ft high by 3 ft wide. Each tank is partitioned by perforated stainless sheet into 35 flow channels, 1 in. wide, each treating 170 gal/hr of AMD. Each unit is thus about 5 ft long for a total reactor volume of 240 ft^3. Table 13 summarizes the capital cost estimation procedure.

Table 13. Capital Cost Analysis for the Packed Bed Reactor Concept (6000 Gal/Hr, 95% Conversion)

Reactor:		
Stainless steel tank	$10,000	Vendor quote
Carbon bed	2,100	50 ¢/lb.
Membrane	1,400	80 ¢/ft^2
	$13,500	

Net capital cost: 2.6¢/1000 gal treated (10% charge rate)

Due to the modular nature of electrochemical devices, the capital charge of 2.6¢/1000 gal is generally applicable to all situations where a conversion of 95% is desired. Table 14 summarizes the capital costs for conversion of 90% and 99%, i.e., for other initial Fe^{2+} concentrations.

Table 14. Capital Charges for the Electrochemical Reactor at Various Conversion Percentages

Conversion, %	Capital Charge, ¢/1000 gal
90	1.9
95	2.6
99	3.8

Not included in Table 14 are the initial costs associated with the AC-DC rectifying and control circuits required for the operation of the oxidation reactor. These costs, which are considered below in the detailed economic evaluation of the proposed AMD treatment scheme, are sensitive to both AMD flow rate and initial Fe^{2+} concentration, as well as to the desired conversion. Since depreciation charges for electrical equipment cannot be directly compared with the costs in Table 14, they are not included at this point.

In addition to the capital charges described above, the only other cost peculiar to the direct oxidation concept is the power cost associated with the oxidation reaction. Labor and maintenance charges are not significant and would not be expected to alter the economics of the overall treatment system.

The additional costs associated with the electrochemical oxidation step can only be compensated by cost reductions in other portions of the treatment scheme. As will be described below, these cost reductions accrue from the elimination of aeration equipment, the use of cheaper limestone rather than lime to precipitate the iron, and a reduction in equipment size and disposal problems due to the denser more rapidly settling sludge produced by the limestone treatment of high ferric content water.

The present technique for treatment of AMD containing substantial Fe^{2+} consists of lime neutralization with concurrent aeration. The resulting sludge is passed into either a clarifier-settler or a settling pond to permit the sludge to thicken. The capital costs of this separation process are the most significant in the AMD treatment system (the choice between a clarifier-settler or a settling pond is usually made on the basis of local topography).

The parameters which permit sizing of the separation equipment (or settling pond) are the settling rate of the sludge and its final solids content. Both of these values can be readily estimated in the laboratory. Fig. 26 presents data on settling rates for limestone treatment of synthetic high ferric mine water. Results are shown for systems containing 0% and 5% ferrous (a total concentration of 1000 mg/ℓ Fe and 2000 mg/ℓ H^+ was maintained). In all cases, the synthetic mine water was neutralized with finely divided $CaCO_3$. For purposes of comparison, and in order to duplicate current practice, similar tests were carried out on a 50% ferrous solution which was precipitated with lime and concurrent aeration. Sludge settling times were determined by allowing the sludge to thicken in graduated cylinders.

As may be expected from data available in the literature, the sludge settling rates observed with limestone treatment of pure ferric mine waters are relatively rapid. A solids content of 6% and a sludge volume of less than 10% of the original AMD volume were observed after 1 hr. Lime neutralization of a mixed ferric/ferrous system produced a much slower settling sludge with a lower solids content. In our experiments, a solids content of 3% and a final sludge volume of 17% were observed after 1 hr. Although literature data vary extensively, limestone sludges are reported to[14] have ultimate settling volumes up to 10 times less than lime sludges.

The results observed with limestone precipitation of a mixed ferrous (50 mg/ℓ) /ferric (950 mg/ℓ) mine water were significantly less attractive. Although the ferrous concentration in the supernate was lowered to 7 mg/ℓ, the sludge produced was of a much lesser density (14% of total solution volume). In order

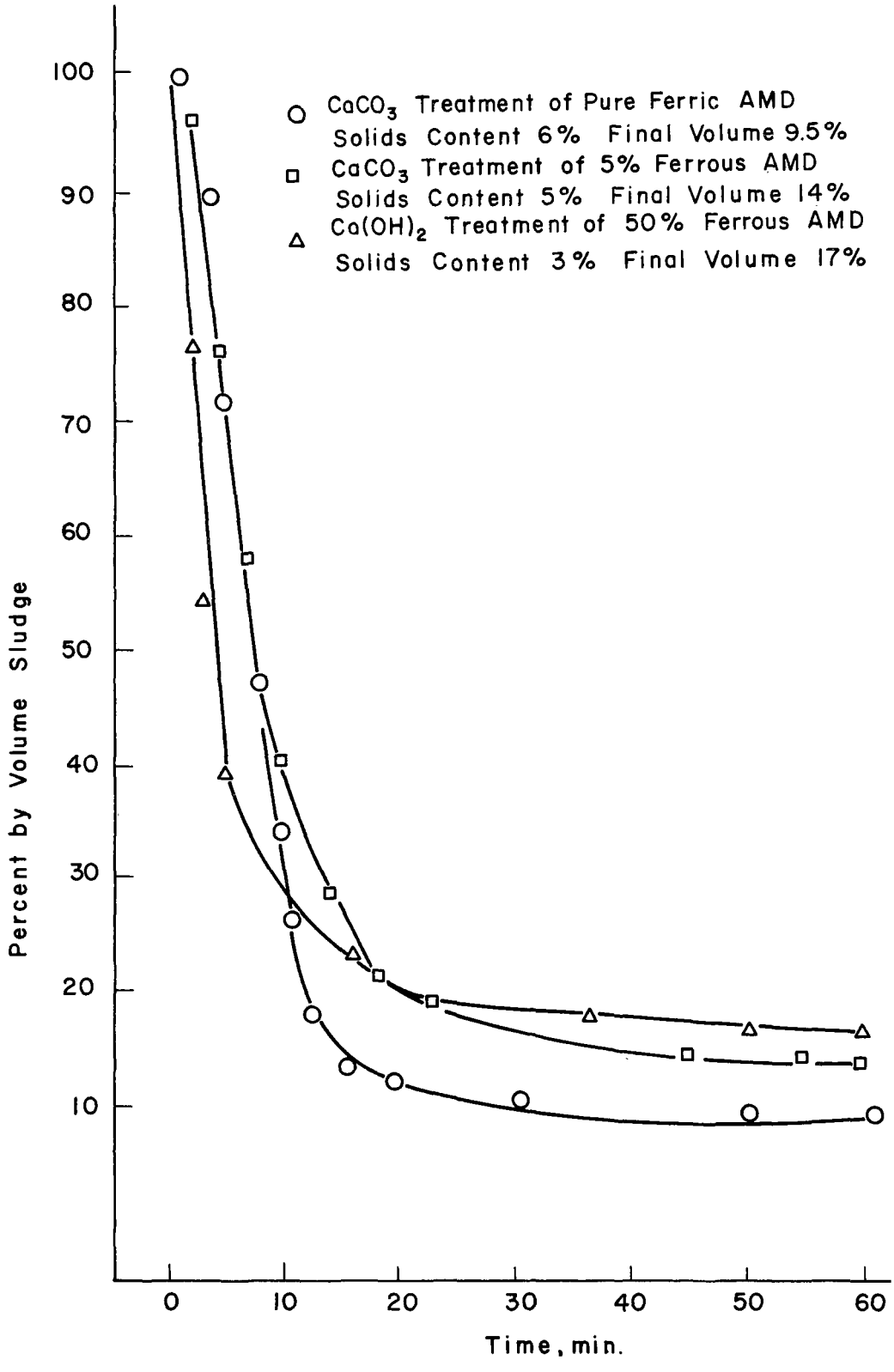

Fig. 26. Settling times of AMD sludges

to ensure meeting stream discharge standards and to minimize sludge disposal volume, the effluent from the oxidation reactor will be designed to contain no more than 5 mg/ℓ Fe^{2+}.

Based on the above data, the clarifier and/or settling pond requirements for limestone treatment of ferric mine water, containing less than 5 mg/ℓ Fe^{2+} may be estimated. Primary settling, performed in a conventional clarifier-settler with a 1 hr residence time, will discharge 10% of the total stream flow to a settling pond/storage basin for final compaction and disposal. The use of a primary clarifier, by reducing the sludge volume and increasing its solids content to 6 to 10% by weight, facilitates sludge disposal in shallow lagoons or abandoned mine shafts. The costs associated with the final storage volume required are, of course, dependent on the initial acidity and iron content of the AMD.

AMD TREATMENT PLANT DESIGN AND ECONOMICS

Since AMD varies widely in composition as well as flow rate, three flows and three ferrous iron concentrations were selected (Table 15) in order to represent a variety of possible situations.

Table 15. AMD Compositions and Flow Rates

Flow Rate, gal/day	Fe^{2+} Concentration, mg/ℓ	Total Acid, mg$CaCO_3$/ℓ
0.25×10^6	1000	2000
1×10^6	500	1000
6×10^6	50	500

If the iron concentration and total acid are not independently varied, a total of 9 design cases must be considered.

The basic treatment scheme is the same in all cases. Under the conservative assumption that no ferrous iron will precipitate during limestone treatment, the oxidation reactor is designed for a final maximum Fe^{2+} concentration of 5 mg/ℓ. Since the flow of mine drainage will vary to some extent, even on a daily basis, a holding pond with a controlled output has been provided. For plants with a low flow rate, the holding pond is also used for AMD storage, thereby reducing labor charges since continuous plant operation would not be necessary.

A limestone slurry is produced by loading a tumbling mill with bulk limestone and providing a flow of water to give the slurry concentration desired. Limestone containing 75% $CaCO_3$ costing $5/ton F.O.B. was used as a basis for estimating equipment size and operating costs.

The AMD from the holding pond is fed to the electrochemical oxidation reactor. Following the oxidation, the limestone slurry is added to the ferric mine water in a simple neutralization reactor. In the absence of ferrous iron, the precipitation should be rapid and in a form favorable to rapid settling. A primary clarifier is used to separate the rapidly settling dilute sludge (about 10% of the total stream flow) from the iron free supernate. The underflow from the primary clarifier is sent to settling lagoons for final compaction and storage.

The economic recovery of the hydrogen produced by the electrochemical oxidation is dependent both on the quantity and iron concentration of the AMD being treated. Location of the AMD site and transportation and packaging costs must also be considered. Although hydrogen generation as a byproduct of AMD treatment can never be economically self sustaining, a significant savings in overall treatments should be obtainable at the high AMD flow rates.

The investment costs for the AMD treatment plants are listed in Table 16. Sizing of the process equipment was based on operating times of 8 hr/day for the 250,000 gal/day rate, 16 hr/day at the 1,000,000 gal/day rate, and continuous operation at 6,000,000 gal/day. Holding pond capacities were adjusted to provide 30 hr retention volume. Process stream flows are thus 41,600 gal/hr, 104,000 gal/hr and 250,000 gal/hr, respectively. Since the capital costs associated with final sludge disposal are too variable to be included without reference to a specific location, this investment requirement has not been included in the preliminary analysis.

The estimated operating expenses (exclusive of final sludge costs) are shown in Table 17. For 500 mg/ℓ Fe^{2+}, the operating costs range from 20¢/1000 gal at 6,000,000 gal/day to 55¢/1000 gal at 250,000 gal/day. Comparable figures for current approaches to AMD treatment are not readily available. In the one case where operating data were available,[15] a lime cost alone of 13¢/1000 gal was reported for a plant treating ~ 3,000,000 gal/day of ~ 200 mg/ℓ Fe^{2+}, 700 mg/ℓ H^+ AMD. Reported values for total treatment costs (including capital charges) appear to range from 20¢ to $2/1000 gal treated.[16]

The proposed approach is strikingly superior in the treatment of badly polluted streams at relatively high flow rates. Conventional lime treatment of a stream containing 2000 mg acidity/ℓ will result in a lime cost alone ~35¢/1000 gal. Electrochemical oxidation, followed by limestone neutralization, results in a reagent cost (treatment power + limestone) of only 19¢/1000 gal

Table 16. Plant Investments

AMD Flow, gal/day	Fe^{2+} Conv, mg/ℓ	Holding Pond, M $	Oxidation Reactor, M $	Electrical Equipment, M $	Limestone Mill, M $	Instru. + Controls, M $	Piping + Tanks M $	Clarifier Settler M $	Equipment Total, M $	Site Preparation, M $	Total Cost, M $
250,000	1000	1.5	160	42	16	3	4	22	251.5	58.5	310
	500	1.5	140	25	6	3	4	22	200	50	250
	50	1.5	70	8.4	4	3	4	22	113	27	140
1,000,000	1000	6	400	84	26	4	5	33	558	142	700
	500	6	351	50	10	4	5	33	459	121	580
	50	6	175	17	6.5	4	5	33	240.5	59.5	300
6,000,000	1000	30	951	168	39	6	6	47	1247	303	1550
	500	30	844	100	15	6	6	47	1048	262	1310
	50	30	422	18	9	6	6	47	538	132	670

at 6,000,000 gal/day. Total process costs for the electrochemical oxidation concept are only 31¢/1000 gallons. Thus, even without consideration of possible savings resulting from the sale of byproduct hydrogen, the direct electrochemical oxidation approach is cheaper than present treatment methods.

Without reference to a specific site location, credits for hydrogen production can only be estimated. Treatment of 1000 gal of AMD containing 500 mg/ℓ Fe^{2+} will result in the generation of 15 ft^3 of hydrogen. Optimized electrolytic hydrogen plants can produce H_2 at about 30¢/100 ft^3. Shipping charges will range from 20¢ to $1/100 ft^3 depending on distance and method.[17] If the byproduct hydrogen can be sold at a credit (after collection and packaging costs) of 40¢/100 ft^3, the credit to the treatment process would be 6¢/1000 gal of AMD treated. At AMD flow rates of 6,000,000 gal/day, this byproduct return would represent a savings of 30% on total treatment costs. For streams containing 1000 mg/ℓ Fe^{2+}, the savings approach 50% of total costs.

Table 17. Estimated Operating Expenses for Direct Electrochemical Oxidation Treatment Plants, ¢/1000 Gal (Lime Treatment Range 20¢ to $2/1000 Gal)

Flow Rate, gal/day	250,000			1,000,000			6,000,000		
Fe^{2+}, mg/ℓ	50	500	1000	50	500	1000	50	500	1000
Acidity, mg/ℓ	500	1000	2000	500	1000	2000	500	1000	2000
Treatment Power, 5 V	0.5	5.3	11	0.5	5.3	11	0.5	5.3	11
Plant Power	3	3	3	3	3	3	3	3	3
Limestone	2	4	8	2	4	8	2	4	8
Labor + Overhead	16	16	16	8	8	8	2	2	2
Depreciation	15	27	34	8.2	16	19	3	6	7
Total Costs	37	55	72	22	36	49	11	20	31

Basis: Power at 1¢/KWhr

Depreciation at 10% of investment

Limestone at $6.67/Ton (100% basis)

Labor + overhead at $5/hr

Plant On-Stream 8, 12 and 24 hours day respectively

SECTION VII

REFERENCES

1. Latimer, W., "Oxidation Potentials," 2nd Ed., Prentice-Hall Publ., N.J. (1952).

2. Hill, R., "Mine Drainage Treatment-State of the Art and Research Needs," U.S. Dept. of the Interior, FWQA Cincinnati, Ohio (December 1968) p. 8.

3. Zittal, H., Miller, F., Anal. Chem., 37, 200 (1965).

4. "Corrosion Resistance of Metals and Alloys," Ed. F.L. LaQue and H. Copson, Reinhold Publ. Corp., N.Y. Chapt. 15 (1963).

5. Levich, V.G., "Physiochemical Hydrodynamics," Ed., N.R. Amundson, Prentice-Hall Inc., Englewood Cliffs, N.J., Chapt. 2 (1962).

6. Schuldiner, S., Roe, R., J. Electroch. Soc., 110, 332 (1963).

7. Potter, E., "Electrochemistry," Cleaver-Hume Press Ltd. Chapt. IV (1961).

8. Riggs, O., Corrosion 19, 180 (1963).

9. Newman, J., Ind and Eng Chem, 60, 4 (1968).

10. Vetter, K., "Electrochemical Kinetics," Academic Press, New York, London, 537 (1967).

11. Klatt, L., Blaedel, W., Anal. Chem., 40, 512 (1968).

12. Saxon, J., Fitton, J., and Vermeulen, T., AICHE Journal, 16, 120 (1970).

13. LeGaff, P., I & E. C., 16, 10 (1969).

14. Lovell, H.L., "The Control and Properties of Sludge Produced From the Treatment of Coal Mine Drainage Water by Neutralization Process," Third Symposium on Coal Mine Drainage (1970), Pittsburg, Pa.

15. Draper, J.C., Third Symposium on Coal Mine Drainage (1970), Pittsburg, Pa.

16. Steinberg, M., Treatment of Acid Mine Drainage by Ozone Oxidation, EPA Contract No. 14-12-838.

17. Hydrogen, "Chemical Week" May 19, 1962.

18. Hamilton and Simpson, Quantitative Chemical Analysis, Macmillan Co., 1964.

19. Treybal, R. E., Mass Transfer Operations, McGraw Hill, 1955.

SECTION VIII

GLOSSARY

N	Normality, i.e., equivalents per liter
n	Number of electrons involved with charge transfer process
F	The Faraday constant (96,500 Asec/equivalent)
D	Diffusion coefficient (cm^2/sec)
r	Radius
v	Kinematic viscosity ($cp/cm^3/g$)
ω	Rotation speed (rad/sec)
C	Bulk concentration of reactive species
i_{lim}	Limiting current
SCE	Saturated calomel electrode (a reference electrode)
E_o	Standard equilibrium potential
E	Reversible electrode potential
R	Gas constant
T	Temperature (°C)
A	Electrode area
δ	Thickness of diffusion layer
$<V>$	Flow velocity

SELECTED WATER RESOURCES ABSTRACTS
INPUT TRANSACTION FORM

1. Report No. | 2. | 3. Accession No. W

4. Title ELECTROCHEMICAL TREATMENT OF ACID MINE WATERS

5. Report Date

6.

8. Performing Organization Report No.

7. Author(s) R. Jasinski
L. Gaines

9. Organization Tyco Laboratories, Inc.
Bear Hill
Waltham, Massachusetts 02154

10. Project No. 14010 FNQ

11. Contract/Grant No. 14-12-859

13. Type of Report and Period Covered

12. Sponsoring Organization

15. Supplementary Notes

16. Abstract Experimental and analytical evaluations of the direct electrochemical oxidation of ferrous acid mine drainage have shown that this approach is economically superior to present lime treatment and aeration methods. Through the use of a packed bed electrode, the size of the oxidation reactor has been reduced to a stage where the capital investment required for this equipment can be recovered by cost reductions in latter treatment stages. These cost savings include:

1. Neutralization with cheaper limestone rather than lime
2. A reduction in sludge settling time due to the better properties of limestone sludges
3. Reduction of sludge disposal volume.

As a bonus, electrolytic hydrogen, produced during electrochemical oxidation should be economically recoverable at the higher AMD treatment rates.

Preliminary economic estimates of total treatment costs indicate a cost range from 11¢ to 72¢/1000 gal, exclusive of hydrogen credits. These costs are much less than those of present treatment approaches which appear to have expense rates of from 20¢ to $2.00/1000 gal treated. In the particular case of a badly polluted stream containing 2000 mg/ℓ of Ca CO_3 acidity, the total treatment cost of 31¢/1000 gallon for the electrochemical oxidation approach is less than the reagent cost alone (~35¢/1000 gal) for conventional lime treatment.

17a. Descriptors

Mine Drainage
Oxidation
Electrolysis

17b. Identifiers

Treatment
Electrochemistry
Electrodes
Permselective membranes

17c. COWRR Field & Group 05D

18. Availability

19. Security Class. (Report)

20. Security Class. (Page)

21. No. of Pages

22. Price

Send To:
WATER RESOURCES SCIENTIFIC INFORMATION CENTER
U.S. DEPARTMENT OF THE INTERIOR
WASHINGTON, D. C. 20240

Abstractor Lewis Gaines | Institution Tyco